Model calculations of doubly closed shell nuclei in CBF theory

III. j-j coupling and isospin dependence.

F.Arias de Saavedra

Departamento de Fisica Moderna, Universidad de Granada,

E-18071 Granada, Spain

G.Co'

Dipartimento di Fisica, Università di Lecce and

INFN, Sezione di Lecce,

I-73100 Lecce, Italy

A.Fabrocini

Dipartimento di Fisica, Università di Pisa and

INFN, Sezione di Pisa,

I-56100 Pisa, Italy

S.Fantoni

Interdisciplinary Laboratory for Advanced Studies (ILAS) and

INFN, Sezione di Trieste,

I-34014 Trieste, Italy

Abstract

Correlated Basis Function theory and Fermi Hypernetted Chain technique are extended to study medium–heavy, doubly closed shell nuclei in j-j coupling scheme, with different single particle wave functions for protons and neutrons and isospin dependent two–body correlations. Central semirealistic interactions are used. Ground state energies, one–body densities, distribution functions and momentum distributions are calculated for ^{12}C, ^{16}O, ^{40}Ca, ^{48}Ca and ^{208}Pb nuclei. The values of the ground state energies provided by isospin dependent correlations are significantly lower than those obtained with isospin independent correlations. In finite nuclear systems, the two–body Euler equations provide correlation functions variationally more effective than those obtained with the same technique in infinite nuclear matter.

1 Introduction

The description of the properties of all nuclear systems, from deuteron to nuclear matter, with a hamiltonian containing realistic two– and three–body potentials is one of the goals of non relativistic nuclear many-body theory [1]. We call realistic those two–body potentials which reproduce the ground state properties of the deuteron and the nucleon–

nucleon scattering data. Three–body forces are generally required to provide a good description of three–body nuclei.

The techniques to solve the Schrödinger equation in few–body systems with these potentials have reached a high degree of sophistication and have produced excellent results [2]. Accurate and reliable technologies have also been developed for infinite nuclear systems, and, nowadays, their results are quite satisfactory [3, 4].

The situation for medium and heavy nuclei is still troublesome. The extension to these nuclei of the Monte Carlo techniques used in few-body systems is hindered by computational difficulties related to the relatively high number of particles involved. In a nucleus like ^{40}Ca the number of spin isospin configurations to be sampled is of the order of the Avogadro's number. On the opposite side, the techniques which made possible accurate numerical studies in infinite nuclear and neutron matters cannot be straightforwardly applied to finite nuclear systems because they do not enjoy translational invariance.

In two previous papers [5, 6] we succeeded in extending Correlated Basis Function (CBF) theory and Fermi Hypernetted Chain (FHNC) cluster summation technique [7] (successfully used to describe nuclear matter properties) to deal with finite Fermi systems. In these works the FHNC theory has been applied to study model, doubly magic nuclei with the same number of protons and neutrons, switching off the Coulomb interaction and using single particle bases in the l–s coupling scheme.

This scheme can be adequate to describe closed shell nuclei up to ^{40}Ca, but it breaks down for heavier nuclei, where the number of neutrons is larger than that of protons. Moreover, while the shell closure for $A \leq 40$ corresponds to that of l–s coupling scheme, for heavier nuclei it is necessary to use a basis with spin-orbit splitting to reproduce the correct sequence of magic numbers.

In the present paper we make a step forward towards a fully microscopic description of all doubly closed shell nuclei. We extend the FHNC formalism to differentiate protons and neutrons and, in addition, to consider single particle bases in a j–j coupling.

In the next section we shall present the modifications of the FHNC equations needed to describe the above nuclear systems.

Nuclei are described as a mixture of neutrons and protons, with possibly different populations. This is reflected by the presence of distribution functions depending on the isospin of the reference nucleons. In a single particle basis generated by a spin–orbit term, the third component of the spin is no longer a good quantum number to describe the single–particle wave functions. For this reason, a new type of statistical link appears in the FHNC equations.

We shall discuss the influence of the aforementioned FHNC modifications on the calculation of the nuclei ground state energy in section 3.

The results of the calculations of binding energies, density and momentum distributions, for various doubly closed shell nuclei are presented in section 4. These calculations have been performed using central nucleon–nucleon interactions (v_4) with spin and isospin dependence and without tensor components. The correlation functions have isospin dependence. Since these interactions and correlations are not yet fully realistic, the results obtained cannot be immediately compared with the experimental data. These are, however, the first, true microscopic calculations in such heavy nucleus as ^{208}Pb and they represent a necessary step towards an *ab initio* description of heavy nuclear systems starting from a realistic nuclear hamiltonian.

2 Extension of the FHNC method

In the framework of CBF theory and along the lines of the formalism presented in [5], the ground state of a nucleus with Z protons and N neutrons ($A = Z + N$) is described by the correlated wave–function:

$$\Psi(1,\ldots,A) = F(1,\ldots,A)\Phi_{N,Z}(1,\ldots,A) \tag{1}$$

where F is an A–body correlation operator we shall specify later. The function $\Phi_{N,Z}$ is a Slater determinant of single particle (s.p.) wave functions $\phi_i^\alpha(i)$ ($\alpha = p,n$) generated by the s.p. hamiltonian

$$h_{sp}^\alpha(i) = -\frac{\hbar^2}{2m}\nabla_i^2 + U^\alpha(i). \tag{2}$$

A proper description of the sequence of magic numbers is achieved only if the s.p. hamiltonian contains a spin–orbit interaction. In this case, the s.p. wave functions are classified in terms of the total angular momentum j and are eigenvectors of j^2 and j_z. We express them as:

$$\phi_{nljm}^{\alpha=p,n}(\mathbf{r}_i) \;=\; R_{nlj}^\alpha(r_i)\sum_{\mu,s}\langle l\mu\frac{1}{2}s \mid jm\rangle Y_{l\mu}(\hat{r}_i)\chi_s(i), \tag{3}$$

where χ_s are the spin wavefuntions, $Y_{l\mu}$ the spherical harmonics and $\langle l\mu 1/2 s \mid jm\rangle$ the Clebsch-Gordan coefficients.

The FHNC equations can be written in terms of the one–body densities and the two–body distribution functions :

$$\rho_1^\alpha(\mathbf{r}) = \langle \Psi^* \sum_{k=1}^{A} \delta(\mathbf{r}-\mathbf{r}_k) P_k^\alpha \Psi \rangle \tag{4}$$

$$\rho_{2,q}^{\alpha\beta}(\mathbf{r},\mathbf{r}') = \langle \Psi^* \sum_{k\neq l=1}^{A} \delta(\mathbf{r}-\mathbf{r}_k) P_k^\alpha \delta(\mathbf{r}'-\mathbf{r}_l) P_l^\beta O_{kl}^q \Psi \rangle \quad q=1,..4 \ , \tag{5}$$

where P_k^α is the projection operator on the $\alpha = p, n$ state of the k–nucleon and we have defined

$$\langle X \rangle = \frac{\int d\tau X}{\int d\tau \mid \Psi \mid^2}, \tag{6}$$

$d\tau$ meaning integration over the spatial coordinates as well as sum over the spins. The index $q = 1, ..4$ labels the operatorial component of $\rho_{2,q}^{\alpha\beta}$. This dependence is the same as that of the v_4 potentials adopted,

$$v_4(1,2) = \sum_{q=1,4} v^{(q)}(r_{12}) O_{12}^q, \tag{7}$$

with $O_{12}^1 = 1, O_{12}^2 = \boldsymbol{\sigma}_1 \cdot \boldsymbol{\sigma}_2, O_{12}^3 = \boldsymbol{\tau}_1 \cdot \boldsymbol{\tau}_2$ and $O_{11}^4 = \boldsymbol{\sigma}_1 \cdot \boldsymbol{\sigma}_2 \boldsymbol{\tau}_1 \cdot \boldsymbol{\tau}_2$.

The uncorrelated density matrices are given by:

$$\begin{aligned} \rho_0^\alpha(\mathbf{r}_1,\mathbf{r}_2) &= \sum_k \phi_k^{\alpha *}(\mathbf{r}_1) \phi_k^\alpha(\mathbf{r}_2) \\ &= \sum_{s,s'} \rho_0^{ss'\alpha}(\mathbf{r}_1,\mathbf{r}_2) \chi_s^\dagger(1) \chi_{s'}(2), \end{aligned} \tag{8}$$

and their spin dependent parts are:

$$\begin{aligned} \rho_0^{ss'\alpha}(\mathbf{r}_1,\mathbf{r}_2) &= \sum_{n,l,j} R_{nlj}^\alpha(r_1) R_{nlj}^\alpha(r_2) \\ & \sum_{\mu,\mu',m} \langle l\mu \frac{1}{2} s \mid jm \rangle \langle l\mu' \frac{1}{2} s' \mid jm \rangle Y_{l\mu}^*(\hat{r}_1) Y_{l\mu'}(\hat{r}_2). \end{aligned} \tag{9}$$

While in the $|l^2 s^2 l_z s_z>$ representation $\rho_0^{ss'\alpha}$ is diagonal in the spin variables [5], in the $|l^2 s^2 j^2 j_z>$ one it depends on the third components of spin (s, s'). The same dependence is also present in the correlated density matrices,

$$\begin{aligned}\rho^{ss'\alpha}(\mathbf{r}_1, \mathbf{r}_{1'}) &= \frac{A}{\langle \Psi \mid \Psi \rangle} \int d^3r_2 \dots d^3r_A \quad \chi_s(1)\chi_\alpha(1) \\ &\quad \Psi^*(1, 2, \dots, A)\Psi(1', 2, \dots, A)\chi^\dagger_{s'}(1')\chi^\dagger_\alpha(1'),\end{aligned} \tag{10}$$

where a sum over all the spin coordinates is implied.

We found convenient to consider separately the uncorrelated density (9) for pairs of particles having either the same or opposite third spin component. For this reason we define

$$\rho^\alpha_{0,P}(\mathbf{r}_1, \mathbf{r}_2) = \frac{1}{8\pi} \sum_{n,l,j} (2j+1) R^\alpha_{nlj}(r_1) R^\alpha_{nlj}(r_2) P_l(\cos\theta_{12}), \tag{11}$$

$$\rho^\alpha_{0,A}(\mathbf{r}_1, \mathbf{r}_2) = \frac{1}{4\pi} \sum_{n,l,j} (-1)^{j-l-1/2} R^\alpha_{nlj}(r_1) R^\alpha_{nlj}(r_2) \sin\theta_{12} P'_l(\cos\theta_{12}), \tag{12}$$

where $P_l(x)$ is the Legendre polynomial of l–th degree and $P'_l(x)$ is its first derivative with respect to x. The function defined in Eq.(11) corresponds to pairs of nucleons with parallel spins, $s = s'$ ($\rho^\alpha_{0,P} = \rho_0^{\frac{1}{2}\frac{1}{2}\alpha} = \rho_0^{-\frac{1}{2}-\frac{1}{2}\alpha}$) . This is the only statistical correlation appearing in l–s coupling. The function defined in Eq.(12), $\rho^\alpha_{0,A} = \rho_0^{\frac{1}{2}-\frac{1}{2}\alpha} = -\rho_0^{-\frac{1}{2}\frac{1}{2}\alpha}$, is instead a new statistical link between nucleons with antiparallel spins, $s = -s'$, due to the j–j coupling. This new function is antisymmetric under the exchange of s with s' and of the spatial coordinates. In all the observables whose mean value we have calculated (energy, density, momentum distribution), we found that the contribution of $\rho^\alpha_{0,P}$ is much larger than that of $\rho^\alpha_{0,A}$. As a matter of fact, if the nucleus is closed in l–s coupling (as for

^{16}O and ^{40}Ca) and no spin–orbit term is included in the s.p. potential, the contribution of $\rho_{0,A}$ vanishes.

The uncorrelated statistical functions appear in the cluster expansion of the two–body distribution functions and of the one–body density matrices forming closed exchange loops. In l–s coupling, all the nucleons involved in the loops must have the same third spin component. In j–j coupling this is no longer true, as there may be statistical links between particles with opposite third components. In general, the contribution from a N–particle exchange loop is given by:

$$(-1)^{N-1}\rho_0^\alpha(\mathbf{r}_1,\mathbf{r}_2)\rho_0^\alpha(\mathbf{r}_2,\mathbf{r}_3)\dots\rho_0^\alpha(\mathbf{r}_N,\mathbf{r}_1) =$$

$$(-1)^{N-1}\sum_{s_1,\dots,s_N}\rho_0^{s_1 s_2\alpha}(\mathbf{r}_1,\mathbf{r}_2)\rho_0^{s_2 s_3\alpha}(\mathbf{r}_2,\mathbf{r}_3)\dots\rho_0^{s_N s_1\alpha}(\mathbf{r}_N,\mathbf{r}_1).$$

3 Energy, density and momentum distribution expectation values

In the previous section we have discussed the modifications induced by j–j coupling and $Z \neq N$ on the uncorrelated density matrix. In this section we will shortly discuss how the FHNC equations change and how the expectation values of energy, density and momentum distribution are calculated.

The structure of the FHNC equations depends on the adopted correlation function. We use an isospin dependent correlation, since we want to distinguish protons from neutrons, and we choose the following form for F, which allows us to consider different correlations for different pairs of nucleons:

$$F(1,\ldots,A) = \prod_{1=i<j}^{A} f_{\alpha\beta}(r_{ij}) P_i^\alpha P_j^\beta. \tag{13}$$

The form of the correlation operator (13), and specifically the fact that the involved operators commute among themselves, allows us to use, in the cluster expansion, the diagrammatic rules presented in Ref.[5], with only slight modifications due to the j–j coupling scheme. Since the system is a mixture of different fermions, the correlated density matrices for pp, pn and nn are different. Furthermore, we have to consider the presence in the cc–FHNC chains of the new statistical link $\rho_{0,A}^\alpha$. The new FHNC expressions of the two–body distribution functions and of the one–body density matrices are given in the Appendices A and B, respectively.

The calculation of the expectation value of the energy has been performed along the same lines followed in Ref. [5].

The evaluation of the kinetic energy has been done using the Jackson–Feenberg identity. This allows us to eliminate terms of the form $(\nabla_i F)(\nabla_i \Phi_0)$, involving three–body operators expectation values [8]. Following the same notation of Ref.[5], we express the kinetic energy as:

$$< T >= T_{JF} = T_F + T_\phi^{(1)} + T_\phi^{(2)} + T_\phi^{(3)}. \tag{14}$$

In the previous equation we have indicated with T_F those terms where the kinetic energy operator acts on the correlation operator F only. Their contribution is given by:

$$T_F = -\frac{\hbar^2}{4m} \sum_{\alpha,\beta} \int d^3r_1 d^3r_2 \rho_{2,1}^{\alpha\beta}(\mathbf{r}_1,\mathbf{r}_2) t[f_{\alpha\beta}(r_{12})], \tag{15}$$

where $t[f]$ has been defined as:

$$t[f(r)] \equiv \frac{1}{f^2(r)}\Big\{ f(r)f''(r) + \frac{2}{r}f(r)f'(r) - f'^2(r)\Big\}. \quad (16)$$

The remaining $T_\phi^{(n=1,2,3)}$ components are the contributions of those terms containing the operator acting on the uncorrelated s.p. wave functions. $T_\phi^{(1)}$ is the sum of the cluster diagrams in which the external point 1, argument of the one–body kinetic energy operator $\hat{T}_1$, is not involved in any exchange (see Eq. 2.24 in [5]). We obtain the expression:

$$T_\phi^{(1)} = -\frac{\hbar^2}{4m}\sum_\alpha \int d^3r_1 \rho_{T1}^\alpha(\mathbf{r}_1)\xi_e^\alpha(\mathbf{r}_1), \quad (17)$$

where ρ_{T1}^α is defined as:

$$\rho_{T1}^\alpha(\mathbf{r}_1) = \sum_i \phi_i^{\alpha *}(\mathbf{r}_1)\nabla_1^2\phi_i^\alpha(\mathbf{r}_1) - \sum_i \nabla_1\phi_i^{\alpha *}(\mathbf{r}_1)\cdot\nabla_1\phi_i^\alpha(\mathbf{r}_1), \quad (18)$$

and ξ_e^α is defined in appendix A.

The other two parts ($T_\phi^{(2,3)}$) contain diagrams where the point 1 belongs to a 2–body ($T_\phi^{(2)}$) or to a $n(>2)$–body ($T_\phi^{(3)}$) exchange loop. We find for $T_\phi^{(2)}$ the expression:

$$T_\phi^{(2)} = \frac{\hbar^2}{4m}\sum_\alpha \int d^3r_1 d^3r_2 \xi_e^\alpha(\mathbf{r}_1)\rho_{T2}^\alpha(\mathbf{r}_1,\mathbf{r}_2)\left[g_{dd}^{\alpha\alpha}(\mathbf{r}_1,\mathbf{r}_2)\xi_e^\alpha(\mathbf{r}_2) - 1\right], \quad (19)$$

where

$$\begin{aligned}\rho_{T2}^\alpha(\mathbf{r}_1,\mathbf{r}_2) \;=\;& \rho_{0,P}^\alpha(\mathbf{r}_1,\mathbf{r}_2)\nabla_1^2\rho_{0,P}^\alpha(\mathbf{r}_1,\mathbf{r}_2) - \nabla_1\rho_{0,P}^\alpha(\mathbf{r}_1,\mathbf{r}_2)\cdot\nabla_1\rho_{0,P}^\alpha(\mathbf{r}_1,\mathbf{r}_2) + \\ & \rho_{0,A}^\alpha(\mathbf{r}_1,\mathbf{r}_2)\nabla_1^2\rho_{0,A}^\alpha(\mathbf{r}_1,\mathbf{r}_2) - \nabla_1\rho_{0,A}^\alpha(\mathbf{r}_1,\mathbf{r}_2)\cdot\nabla_1\rho_{0,A}^\alpha(\mathbf{r}_1,\mathbf{r}_2). \quad (20)\end{aligned}$$

All the FHNC quantities introduced in the above equations are defined in appendix C.

The evaluation of $T_\phi^{(3)}$ requires the knowledge of the three–body distribution functions, but its leading term ($T_\phi^{(3,2)}$) is a function of two–body dressed FHNC quantities [5]. $T_\phi^{(3,2)}$

is given by:

$$T_{\phi}^{(3,2)} = -\frac{\hbar^2}{2m} \sum_{\alpha} \int d^3r_1 d^3r_2 \left[\rho_{T3,P}^{\alpha}(\mathbf{r}_1,\mathbf{r}_2) H_{cc,P}^{\alpha}(\mathbf{r}_1,\mathbf{r}_2) + \rho_{T3,A}^{\alpha}(\mathbf{r}_1,\mathbf{r}_2) H_{cc,A}^{\alpha}(\mathbf{r}_1,\mathbf{r}_2) \right], \quad (21)$$

where

$$\begin{aligned} H_{cc,X}^{\alpha}(\mathbf{r}_1,\mathbf{r}_2) &= \xi_e^{\alpha}(r_1) \{ \xi_e^{\alpha}(r_2) [(g_{dd}^{\alpha\alpha}(\mathbf{r}_1,\mathbf{r}_2) - 1) N_{cc,X}^{\alpha}(\mathbf{r}_1,\mathbf{r}_2) + N_{cc,X}^{(x)\alpha}(\mathbf{r}_1,\mathbf{r}_2)] \\ &+ (\xi_e^{\alpha}(r_2) - 1) N_{cc,X}^{(\rho)\alpha}(\mathbf{r}_1,\mathbf{r}_2) + \xi_e^{\alpha}(r_2) g_{dd}^{\alpha\alpha}(\mathbf{r}_1,\mathbf{r}_2) E_{cc,X}^{\alpha}(\mathbf{r}_1,\mathbf{r}_2) \}, \quad (22) \end{aligned}$$

with $X = P, A$. The remaining term $T_{\phi}^{(3,3)}$ contains a three-body operator and it is known to be negligible, both in nuclear matter and N=Z nuclei [5]. Therefore, it has been neglected.

The center of mass kinetic energy, T_{cm}, has to be subtracted from $< H >$ to get the energy mean value E. T_{cm} is given by:

$$T_{cm} = -\frac{\hbar^2}{4mA} \sum_{\alpha=p,n} \int d^3r_1 \left(\rho_{T1}^{\alpha}(\mathbf{r}_1) - \int d^3r_2 \rho_{T4}^{\alpha}(\mathbf{r}_1,\mathbf{r}_2) \right). \quad (23)$$

The expressions of the ρ_{Tx}^{α} functions are given in appendix C.

The potential energy $< V >$ may be written as:

$$< V >= \frac{1}{2} \sum_{\alpha,\beta=p,n} \int d^3r_1 d^3r_2 \sum_{q=1,4} v^{(q)}(r_{12}) \rho_{2,q}^{\alpha\beta}(\mathbf{r}_1,\mathbf{r}_2). \quad (24)$$

The two–body distribution functions can be decomposed into a direct part, summing those contributions where the particles 1 and 2 do no belong to the same exchange loop, and two exchange parts, containing diagrams where the two nucleons are involved in the same loop with identical ($\rho_{exc,P}$) or opposite ($\rho_{exc,A}$) third spin components:

$$\rho_{2,q}^{\alpha\beta}(\mathbf{r}_1,\mathbf{r}_2) = a_q^{\alpha\beta} \rho_{dir}^{\alpha\beta}(\mathbf{r}_1,\mathbf{r}_2) + b_q^{\alpha\beta} \rho_{exc,P}^{\alpha\beta}(\mathbf{r}_1,\mathbf{r}_2) + c_q^{\alpha\beta} \rho_{exc,A}^{\alpha\beta}(\mathbf{r}_1,\mathbf{r}_2). \quad (25)$$

The a, b and c factors are given in Tab.1. The expressions for ρ_{dir} and $\rho_{exc,X}$ are:

$$\begin{aligned}
\rho^{\alpha\beta}_{dir}(\mathbf{r}_1,\mathbf{r}_2) &= \xi^{\alpha}_{d}(\mathbf{r}_1)(\xi^{\beta}_{d}(\mathbf{r}_2)g^{\alpha\beta}_{dd}(\mathbf{r}_1,\mathbf{r}_2)+\xi^{\beta}_{e}(\mathbf{r}_2)g^{\alpha\beta}_{de}(\mathbf{r}_1,\mathbf{r}_2))+ \\
& \xi^{\alpha}_{e}(\mathbf{r}_1)\xi^{\beta}_{d}(\mathbf{r}_2)g^{\alpha\beta}_{ed}(\mathbf{r}_1,\mathbf{r}_2)+ \\
& \xi^{\alpha}_{e}(\mathbf{r}_1)\xi^{\beta}_{e}(\mathbf{r}_2)g^{\alpha\beta}_{dd}(\mathbf{r}_1,\mathbf{r}_2)\Big[N^{\alpha\beta}_{ee}(\mathbf{r}_1,\mathbf{r}_2)+E^{\alpha\beta}_{ee,dir}(\mathbf{r}_1,\mathbf{r}_2)+ \\
& (N^{\alpha\beta}_{de}(\mathbf{r}_1,\mathbf{r}_2)+E^{\alpha\beta}_{de}(\mathbf{r}_1,\mathbf{r}_2))(N^{\alpha\beta}_{ed}(\mathbf{r}_1,\mathbf{r}_2)+E^{\alpha\beta}_{ed}(\mathbf{r}_1,\mathbf{r}_2))\Big], \qquad (26) \\
\rho^{\alpha\beta}_{exc,X}(\mathbf{r}_1,\mathbf{r}_2) &= \xi^{\alpha}_{e}(\mathbf{r}_1)\xi^{\beta}_{e}(\mathbf{r}_2)g^{\alpha\beta}_{dd}(\mathbf{r}_1,\mathbf{r}_2)\Big[E^{\alpha\beta}_{ee,exc,X}(\mathbf{r}_1,\mathbf{r}_2)- \\
& 2(N^{\alpha}_{cc,X}(\mathbf{r}_1,\mathbf{r}_2)+E^{\alpha}_{cc,X}(\mathbf{r}_1,\mathbf{r}_2)-\rho^{\alpha}_{0,X}(\mathbf{r}_1,\mathbf{r}_2)) \\
& (N^{\beta}_{cc,X}(\mathbf{r}_1,\mathbf{r}_2)+E^{\beta}_{cc,X}(\mathbf{r}_1,\mathbf{r}_2)-\rho^{\beta}_{0,X}(\mathbf{r}_1,\mathbf{r}_2))\Big]. \qquad (27)
\end{aligned}$$

We consider also the contribution of the Coulomb interaction acting between the protons. Its expectation value is:

$$< V_c >= \frac{1}{2}\int d^3r_1 d^3r_2 \frac{e^2}{r_{12}}\rho^{pp}_{2,1}(\mathbf{r}_1,\mathbf{r}_2). \qquad (28)$$

The mean value of the energy is then given by $E = T_{JF}+ < V > + < V_c > - T_{cm}$.

Since the one–body density matrices depend on the third components of the spin (Eq.(10)), also the momentum distributions have this dependence :

$$n^{ss'\alpha}(k) = \frac{1}{A}\int d^3r_1 d^3r_{1'} e^{i\mathbf{k}\cdot(\mathbf{r}_1-\mathbf{r}_{1'})}\rho^{ss'\alpha}(\mathbf{r}_1,\mathbf{r}_{1'}). \qquad (29)$$

The spin averaged momentum distribution, summed over all the possible spin components, is:

$$n^{\alpha}(k) = \sum_{s,s'} n^{ss'\alpha}(k), \qquad (30)$$

and, in the following, we shall always refer to the momentum distribution as defined by Eq.(30). The FHNC derivation of the one–body density matrices are given in appendix B.

We conclude this section by listing some sum rules (SR) that must be satisfied by the densities, the two–body distribution functions and the momentum distributions. They are particularly relevant since provide information about the accuracy of the approximations used to solve the FHNC equations.

For the densities and the distribution functions, the following SR's hold:

$$
\begin{aligned}
S_p &= \frac{1}{Z}\int d^3r\rho_1^p(\mathbf{r}) = 1, && (31)\\
S_n &= \frac{1}{N}\int d^3r\rho_1^n(\mathbf{r}) = 1, && (32)\\
S_{pp} &= \frac{1}{Z(Z-1)}\int d^3r_1d^3r_2\rho_{2,1}^{pp}(\mathbf{r}_1,\mathbf{r}_2) = 1, && (33)\\
S_{np(pn)} &= \frac{1}{ZN}\int d^3r_1d^3r_2\rho_{2,1}^{np(pn)}(\mathbf{r}_1,\mathbf{r}_2) = 1, && (34)\\
S_{nn} &= \frac{1}{N(N-1)}\int d^3r_1d^3r_2\rho_{2,1}^{nn}(\mathbf{r}_1,\mathbf{r}_2) = 1. && (35)
\end{aligned}
$$

In nuclei, where the levels with the same value of the orbital angular momentum are saturated (as ^{16}O and ^{40}Ca), the spin–SR S_σ,

$$
S_\sigma = \frac{1}{3A}\int d^3r_1d^3r\;[\rho_{2,2}^{pp}(\mathbf{r}_1,\mathbf{r}_2) + \rho_{2,2}^{nn}(\mathbf{r}_1,\mathbf{r}_2)], \tag{36}
$$

has to satisfy the condition $S_\sigma = -1$. This is no longer true for the nuclei ^{12}C, ^{48}Ca and ^{208}Pb. However, as the correlations do not contain spin flip terms, S_σ in the correlated nucleus must have the same value as in the uncorrelated one ($S_\sigma^{corr} = S_\sigma^{unc}$).

The momentum distributions must obey the zeroth momentum SR:

$$MD_0^\alpha = \frac{1}{(2\pi)^3} \int d^3k n^\alpha(k) = x_\alpha, \tag{37}$$

where x_α is the proton ($x_p = Z/A$) or neutron fraction ($x_n = N/A$), and the second momentum SR:

$$MD_2 = \frac{\hbar^2}{2m(2\pi)^3} \int d^3k k^2 A[n^p(k) + n^n(k)] =< T > . \tag{38}$$

4 Results

We have applied the theoretical framework presented in the previous sections to the study of the ground state properties of the ^{12}C, ^{16}O, ^{40}Ca, ^{48}Ca and ^{208}Pb nuclei.

Our calculations have been done using two different kinds of correlation functions. One has a gaussian behaviour:

$$f^G_{\alpha\beta}(r) = 1 - A_{\alpha\beta} \exp(-B_{\alpha\beta} r^2), \tag{39}$$

where $A_{\alpha\beta}$ and $B_{\alpha\beta}$ are taken as variational parameters, fixed by minimizing the FHNC energy.

The second correlation function is obtained by the minimization of the energy at the second order of the cluster expansion, $< H_2 >$, with

$$\begin{aligned} < H_2 > &= -\frac{\hbar^2}{4m} \sum_{\alpha=p,n} \int d^3r_1 \left(\rho^\alpha_{T1}(\mathbf{r}_1) + \int d\mathbf{r}_2 \rho^\alpha_{T2}(\mathbf{r}_1, \mathbf{r}_2) \right) + \\ &\sum_{\alpha,\beta=p,n} \int d^3r_1 d^3r_2 \left[Q_{\alpha\beta}(\mathbf{r}_1, \mathbf{r}_2) f^2_{\alpha\beta}(r_{12}) - P_{\alpha\beta}(\mathbf{r}_1, \mathbf{r}_2) \left(f_{\alpha\beta}(r_{12}) \nabla^2_{12} f_{\alpha\beta}(r_{12}) - (f'_{\alpha\beta}(r_{12}))^2 \right) \right] . \end{aligned} \tag{40}$$

The solution of $\delta < H_2 > /\delta f_{\alpha\beta} = 0$ provides the Euler Correlations $f^E_{\alpha\beta}$.

The quantities $Q(P)_{\alpha\beta}$ are generalizations to the isospin dependent case of those of Ref.[5]:

$$
\begin{aligned}
Q_{\alpha\beta}(\mathbf{r}_1,\mathbf{r}_2) &= \delta_{\alpha\beta}\frac{\hbar^2}{4m}\rho^{\alpha}_{T2}(\mathbf{r}_1,\mathbf{r}_2) + \frac{1}{2}\rho^{\alpha}_0(\mathbf{r}_1)\rho^{\beta}_0(\mathbf{r}_2)V^{\alpha\beta}_{dir}(r_{12}) - \qquad (41)\\
&\left[\rho^{\alpha}_{0,P}(\mathbf{r}_1,\mathbf{r}_2)\rho^{\beta}_{0,P}(\mathbf{r}_1,\mathbf{r}_2)V^{\alpha\beta}_{exc,P}(r_{12}) + \rho^{\alpha}_{0,A}(\mathbf{r}_1,\mathbf{r}_2)\rho^{\beta}_{0,A}(\mathbf{r}_1,\mathbf{r}_2)V^{\alpha\beta}_{exc,A}(r_{12})\right],\\
P_{\alpha\beta}(\mathbf{r}_1,\mathbf{r}_2) &= \frac{\hbar^2}{4m}\left\{\rho^{\alpha}_0(\mathbf{r}_1)\rho^{\beta}_0(\mathbf{r}_2) - 2\delta_{\alpha\beta}\left[(\rho^{\alpha}_{0,P}(\mathbf{r}_1,\mathbf{r}_2))^2 + (\rho^{\alpha}_{0,A}(\mathbf{r}_1,\mathbf{r}_2))^2\right]\right\}, \qquad (42)
\end{aligned}
$$

where:

$$
\begin{aligned}
V^{\alpha\beta}_{dir}(r_{12}) &= \delta_{\alpha\beta}[v^{(1)}(r_{12}) + v^{(3)}(r_{12})] + (1-\delta_{\alpha\beta})[v^{(1)}(r_{12}) - v^{(3)}(r_{12})], \qquad (43)\\
V^{\alpha\beta}_{exc,P}(r_{12}) &= -2\delta_{\alpha\beta}[v^{(1)}(r_{12}) + v^{(3)}(r_{12}) + 3v^{(2)}(r_{12}) + 3v^{(4)}(r_{12})] - \qquad (44)\\
&4(1-\delta_{\alpha\beta})[v^{(3)}(r_{12}) + 3v^{(4)}(r_{12})],\\
V^{\alpha\beta}_{exc,A}(r_{12}) &= -2\delta_{\alpha\beta}[v^{(1)}(r_{12}) + v^{(3)}(r_{12}) - v^{(2)}(r_{12}) - v^{(4)}(r_{12})] - \qquad (45)\\
&4(1-\delta_{\alpha\beta})[v^{(3)}(r_{12}) - v^{(4)}(r_{12})].
\end{aligned}
$$

The contributions to $< H_2 >$ decouple in the $(\alpha\beta)$ channels, so the minimizations are independently performed for each component. The corresponding Euler–Lagrange equations are:

$$
u''_{\alpha\beta}(r) - \overline{V}_{\alpha\beta}(r)u_{\alpha\beta}(r) = \lambda_{\alpha\beta}u_{\alpha\beta}(r), \qquad (46)
$$

with:

$$u_{\alpha\beta}(r) = r\sqrt{\overline{P}_{\alpha\beta}(r)}f_{\alpha\beta}(r) \tag{47}$$

$$\overline{V}_{\alpha\beta}(r), = \frac{1}{4\overline{P}_{\alpha\beta}(r)}\left[\nabla^2\overline{P}_{\alpha\beta}(r) + 2\overline{Q}_{\alpha\beta}(r) + \frac{\overline{P}'_{\alpha\beta}(r)^2}{\overline{P}_{\alpha\beta}(r)}\right]. \tag{48}$$

The $\overline{P}_{\alpha\beta}$ and $\overline{Q}_{\alpha\beta}$ terms are obtained by integrating $P_{\alpha\beta}(\mathbf{r}_1, \mathbf{r}_2)$ and $Q_{\alpha\beta}(\mathbf{r}_1, \mathbf{r}_2)$ over $\mathbf{r}_1$ and $\mathbf{r}_2$ and keeping r_{12} fixed:

$$\overline{X}(r_{12}) = \frac{1}{r_{12}}\int_0^\infty dr_1 r_1 \int_{|r_{12}-r_1|}^{r_{12}+r_1} dr_2 r_2 X(r_1, r_2, r_{12}), \tag{49}$$

where X can be either P or Q.

Eqs. (46) are solved under the constraints:

$$f_{\alpha\beta}(r \geq d_{\alpha\beta}) = 1 \qquad\qquad f'_{\alpha\beta}(r \geq d_{\alpha\beta}) = 0, \tag{50}$$

where the healing distances $d_{\alpha\beta}$ are variational parameters. The same value for all the healing distances ($d_{\alpha\beta} = d$) has been used in this paper.

In some calculations, we have also adopted the Average Correlation Approximation (ACA), consisting in using an unique correlation, independent on the isospin of the nucleons, for both types of correlations, either gaussian or Euler.

For the gaussian correlation, ACA simply consists in using the same values of the A and B constants for each channel.

The ACA Euler equation is immediately obtained by summing over the α, β effective potentials. The resulting equation is:

$$u''(r) - \overline{V}(r)u(r) = \lambda u(r), \tag{51}$$

where:

$$u(r) = r\sqrt{\overline{P}(r)}f(r), \tag{52}$$

$$\overline{V}(r) = \frac{1}{4\overline{P}(r)}\left[\nabla^2\overline{P}(r) + 2\overline{Q}(r) + \frac{\overline{P}'(r)^2}{\overline{P}(r)}\right], \tag{53}$$

$$\overline{P}(r) = \sum_{\alpha\beta}\overline{P}_{\alpha\beta}(r), \tag{54}$$

$$\overline{Q}(r) = \sum_{\alpha\beta}\overline{Q}_{\alpha\beta}(r). \tag{55}$$

The second ingredient of the calculations is the set of s.p. wave functions. In this paper, they have always been generated by a mean field potential of Woods–Saxon type:

$$V_{WS}(\mathbf{r}) = \frac{-V_0}{1+e^{(r-R)/a}} + \left(\frac{\hbar}{m_\pi c}\right)^2 \frac{1}{r}\frac{d}{dr}\left(\frac{-V_{ls}}{1+e^{(r-R)/a}}\right)\mathbf{l}\cdot\boldsymbol{\sigma} + V_{Coul}, \tag{56}$$

where m_π is the pion mass.

As a test of accuracy of the calculations, we show in Tab.2 the level of exhaustion of the previously discussed densities and distribution functions SR's. They have been calculated in the FHNC/0 approximation, consisting in neglecting the elementary (or bridge) diagrams. These diagrams, designed as $E^{\alpha\beta}_{xy}$ in Appendix A, cannot be summed in a closed way by FHNC. Therefore, they are usually neglected. In some cases, their contribution is approximated by considering only a few low order terms. The seemingly crude FHNC/0 approximation has been shown to be accurate in relatively low density systems as nuclei and nuclear matter [3], whereas the elementary diagrams become increasingly important in high density systems as liquid atomic Helium [10]. On the other side, it has already been pointed out that the SR's are evaluated just to ascertain the degree of accuracy of the approximations employed in solving the FHNC equations. In the following, we shall always use FHNC/0, unless differently stated.

The results shown in Tab.2 have been obtained with the parameters of the ACA calculations of Tab.5, whose details will be discussed later. In the non ACA case, the accuracy is substantially the same. The SR's are very well satisfied for all the medium–heavy nuclei. The worse situation is met in ^{208}Pb, but the error remains less than 2%.

In the last two rows of the Table we show the ratios between the values of the spin SR of Eq.(36) obtained in the correlated system and that obtained in the uncorrelated one ($S_\sigma^{corr}/S_\sigma^{unc}$). In the row labelled $S_{\sigma,0}$ the correlated value has been evaluated in FHNC/0, while in the row labelled $S_{\sigma,1}$ the contribution of the first order exchange elementary diagram has been included (see Ref.[5] for a more extensive discussion of this point). This last approximation has been termed as FHNC–1. In agreement with the findings of Ref. [5], Tab.2 shows that the FHNC–1 approximation substantially improves the accuracy of the calculated spin sum rules with respect to FHNC/0.

A first set of calculations has been performed to investigate the relevance of the j–j coupling, of the Coulomb interaction and of the separate treatment of protons and neutrons. In order to have a better control on their contributions, we have used the same set of Woods-Saxon parameters, identical for protons and neutrons and without spin–orbit term. In addition, we have taken the same s.p. potentials in ^{12}C and ^{16}O and for the Ca isotopes, as shown in Tab.3, to investigate the influence of the unsaturated l shells. The semi–realistic S3 interaction of Afnan and Tang [11], supplemented in the odd channels with the repulsive interaction given by the repulsive terms of the even channels as discussed in Ref. [12], has been adopted in conjunction with the Euler ACA correlation function.

In Tab.4 we present the results of the ground state energies. Column F1 has been obtained by switching off the Coulomb interaction and the statistical correlation arising from the j–j coupling, Eq.(12). Its effect can be seen by comparing the results of column F1 with those of column F2, where the j–j coupling has been reinstated. Only ^{12}C, ^{48}Ca and ^{208}Pb nuclei, which have some unsaturated l shell, are affected by this correlation and its influence turns out to be rather small.

The F3 column shows the results obtained including the Coulomb interaction in the two–body hamiltonian. The contribution of the nuclear interaction (V in the Table) to the binding energy is about the same for ^{40}Ca, ^{48}Ca and ^{208}Pb. These nuclei are large enough to allow the nuclear interaction to saturate. The contribution of the Coulomb interaction V_c, because of the infinite range of the force, increases like the number of proton pairs, as expected.

The results of the F4 column have been obtained by inserting the Coulomb potential also in the mean field. We have used the potential generated by an uniform spherical charge distribution. Other choices did not make any difference from the numerical point of view.

A fully implemented variational principle would require performing the minimization of the energy functional respect to both the s.p. wave functions and the correlation function parameters. This implies a large parameter space minimization. Because the requested numerical effort is heavy, and also because we are not yet considering fully realistic interactions, the set of single particle wave functions has been kept fixed and the minimization has been done only respect to the correlation function.

Moreover, for all the columns of Tab.4 we have used the same correlations (obtained by minimizing the F1 energies). Therefore, we cannot draw any definite conclusion on whether the l–s coupling is or is not variationally preferred with respect to the j–j coupling, except that we find very small differences in the two cases. Similarly, we should not be surprised by the fact that the inclusion of the Coulomb effects in the wave function (column F4) does not seem to lower the energies with respect to their perturbative estimates of column F3.

In all the calculations we shall discuss henceforth the s.p. wave functions have been generated by Wood-Saxon potentials whose parameters, given in Tab.5, are taken from literature [9], and have been fixed to reproduce the s.p. energies around the Fermi surface and the rms charge radii.

Table 6 gives the results obtained with the S3 interaction and various correlation functions. The EU rows show the results with the isospin dependent Euler correlation function, the ACA rows those with the ACA Euler correlation and the G rows those with the gaussian ACA correlation. The columns present the contributions of the various terms building up the average value of the binding energy. The binding energies per nucleon, E/A, have been calculated by subtracting the center of mass energy. In the last column the healing distances, for the minimum of the energy with the Euler correlations, are given. Note that the EU calculations have been performed using the same value of the healing distance for all the isospin channels.

For all the nuclei we have considered, the isospin dependent correlation function results to be variationally preferred respect to the simpler ACA functions. This is mainly produced by a large decrease of the potential energy, which overcompensates the increase of the kinetic energy. The poorest choice is the ACA gaussian one.

The correlation functions used in the ACA Euler and gaussian calculations of Tab.6 are shown in Fig.1. They are very similar in all the nuclei we have studied and all the finite system Euler correlations overshoot one.

Also in the isospin dependent case, where f^{pp}, f^{nn} and f^{np} are different even if we assume the same healing distance for all of them, the correlations do not show a strong dependence on the type of nucleus considered. This is due to the fact that the correlations are mostly sensitive to the short range behaviour of the nuclear interaction. Fig.2 compares the isospin dependent Euler correlations with the ACA Euler ones for ^{12}C and ^{208}Pb. f^{pp} and f^{nn} are close to f^{ACA}, but f^{np} shows large differences. This rich isospin structure is responsible for the better variational behaviour of the correlation.

It is interesting to compare the finite nuclei Euler correlations with those of infinite nuclear matter. In this case, we put $f^{nn} = f^{pp} = f_{NM}^{T=1}$ and $f^{np} = \frac{1}{4}[3f_{NM}^{T=1} + f_{NM}^{T=0}]$, where $T = 0, 1$ is the total isospin. The nuclear matter correlations are always smaller than one, therefore the overshooting feature of the Euler correlations in the nuclei seems to be ascribed to the finite nature of the systems. Nuclear matter correlations have been often used in finite nuclei [13] on the assumption that their short range behaviour is little affected by the size of the system. However, we find non–negligible differences and improved energies by using correlations generated by the finite system Euler equations. For instance, in ^{12}C f_{NM}^{T} gives $E/A = -2.12MeV$ at $d = 2.0fm$, to be compared with the $E/A = -4.65MeV$ value of the Euler correlation.

The proton one–body densities, $\rho_1^p(\mathbf{r})$, calculated with the Euler and gaussian correlations are given in Fig.3 for ^{12}C, ^{16}O and the Calcium isotopes and Fig.5 for ^{208}Pb, and compared with their uncorrelated counterparts, $\rho_0^p(\mathbf{r})$, (full lines). The dotted curves have been obtained with the gaussian–ACA correlations and all of them are lower than the uncorrelated densities at low r–values. On the other hand, those obtained in the Euler (dashed–dotted lines) and ACA Euler (dashed lines) calculations are larger than $\rho_0^p(\mathbf{r})$. This indicates that the correlation effect on $\rho_1^p(\mathbf{r})$ at small distances may strongly depend on the type of correlation employed. The results of the figures have been obtained for those values of the variational parameters giving the minimum energy. We found correlated densities smaller than $\rho_0^p(\mathbf{r})$ in the nuclear center when we used values of the healing distance far from those producing the energy minima.

Similar results have been obtained for the neutrons density distributions.

In order to check the validity of our approximations and their sensitivity to the choice of the nucleon–nucleon interaction, we have performed ACA Euler calculations with the Brink and Boeker B1 central potential[14]. The B1 potential is not a microscopic one, as it does not fit two–body data. It is an effective interaction which reproduces the nuclear matter and ^{4}He binding energies in Hartree-Fock theory. This potential has been used in Ref.[5] to compare its FHNC results with the available, exact Variational Monte Carlo calculations in ^{16}O.

The accuracy of the SR's for the B1 potential is the same as for S3. The ground state expectation values of the various terms of the hamiltonian are shown in Tab. 7. Also in B1 case, the correlation functions, shown in Fig.6, are very similar for all the nuclei considered. However, some differences from those obtained with the S3 interaction are present. The B1 correlations have a value of about 0.55 at $r = 0$ fm, versus the 0.37 value of the S3 case. In addition, the overshooting is rather small.

The differences in the correlation functions have some consequences on the proton density distributions, shown in Figs.3 and 5 by the dashed–doubly–dotted lines. All these distributions are smaller than the uncorrelated ones, in contrast with the ACA Euler results with S3.

We have studied the effect on the energy of the insertion of the dressed, lowest order exchange elementary diagrams in FHNC–1. The results are summarized in Tab.8, where the FHNC–1 energies per nucleon (columns E_1) obtained with the Euler–ACA correlations for both S3 and B1 interactions are given. In addition we give the percentile deviations Δ from the FHNC/0 energies:

$$\Delta = 100 \frac{E_0 - E_1}{E_0} \tag{57}$$

where E_1 and E_0 are the FHNC–1 and FHNC/0 energies respectively.

Confirming the finding of Ref.[5], E_1 is always higher than E_0. Moreover, the influence of this class of elementary diagram becomes small in large nuclei, in agreement with nuclear matter results [15].

The proton MDs, $n^p(k)$, obtained for S3 are shown in Fig.4 for ^{12}C,^{16}O,^{40}Ca and ^{48}Ca nuclei, and, in the lower panel of Fig.5 for ^{208}Pb. In the same figures we show the uncorrelated distributions (full lines) and $n^p(k)$ for the B1 model with the ACA Euler correlations. The MD sum rules of Eqs.(37,38) are given in Tab.(9) for different wave functions. The MD_0^α sum rules are very well satisfied, with errors less than 1%, except one single case. The MD_2 sum rules are also well satisfied, even if with a lower accuracy. However, for the best variational case (the Euler correlation) the error in MD_2 is, at most, about 5%.

All the FHNC results show the same known features: the correlated results are orders of magnitude larger that the uncorrelated ones at high momentum values. In particular, the isospin dependent correlations enhance the tails of the MDs more than the Jastrow, isospin independent choice. This result is in line with the findings of Ref.[6], where the effect of state dependent correlations (having spin, isospin and tensor components) was estimated, from CBF Nuclear Matter calculations, in a suitable Local Density Approximation and compared with a Jastrow finite nuclei FHNC evaluation of $n(k)$ in N=Z nuclei. State dependence was found to increase the tails of the MDs of about one order of magnitude more than the Jastrow correlations. The enhancement found here is somewhat smaller. However, a consistent FHNC approach, to deal with nuclear matter type correlations, is called for before a quantitative an definite answer may be given.

5 Conclusions

This work represents a further step towards a fully microscopical description of medium–heavy nuclei. For the first time we have performed FHNC calculations for medium and heavy finite nuclear systems. The calculations have been done using different s.p. wave functions for protons and neutrons, in j–j coupling, isospin dependent correlations and semirealistic, central potentials. The Coulomb interaction has been also considered.

The extension of the FHNC equations of Refs.[5, 6] is not straightforward because, due to the j–j coupling scheme, a new type of statistical link appears.

We have used the central S3, Afnan and Tang, and B1, Brink and Boeker, interactions. The s.p. wave functions have been generated by Woods–Saxon potentials, whose parameters have been taken from literature.

A detailed analysis of the influence of the j–j statistical correlations on the FHNC equations has been presented. Their contribution is rather small, while the effect of the Coulomb interaction, especially for heavy nuclei, turns out to be relevant.

Both isospin dependent and independent correlation functions have been used. The first ones allow us to distinguish between *pp nn* and *np* channels. In all the nuclei considered we have found that the *pp* and *nn* correlations are quite close to each other, while the *np* correlation shows pronounced differences. This marked isospin structure appears to be variationally preferred, as it lowers the ground state energies considerably with respect to the results obtained with isospin independent correlations.

At the variational minima, the correlation functions do not strongly depend on the nucleus considered. However, they show an intermediate range structure, not present in the optimal FHNC correlations of infinite, symmetric nuclear matter. This difference has large effects on the energies and the density distributions.

The accuracy of the FHNC/0 and FHNC–1 approximations has been studied by examining the density and distribution functions sum rules. FHNC/0 is found rather accurate, the largest error being less than 2% in the scalar sum rules. The inclusion of the lowest order, exchange elementary diagram, in FHNC–1, lowers the error in the spin sum rules to less than 1%. The FHNC–1 correction is also relevant in the ground state energy, because the adopted potentials have large Majorana parts [5]. However, its contribution is negligible for large mass nuclei, as ^{208}Pb.

As far as the matter density is concerned, it appears that, given a chosen s.p. structure, the correlations may largely and differently modify the density distribution. The results we have presented are however related to energy minima obtained by performing variations of the correlation functions only. Before drawing any sensible conclusion one should include tha correlations in a fully consistent scheme. In our case, this means to perform the energy minimization by also varying the mean field parameters.

The momentum distributions have been calculated within the FHNC/0 scheme and the sum rules analysis shows that its accuracy is actually very satisfactory. Short range correlations produce high momentum tails, absent in an independent particle model. The momentum distributions calculated with state dependent correlations show tails higher than those produced by Jastrow, state dependent correlations.

In this paper, we have shown, that it is possible to treat accurately doubly closed shell nuclei in the j–j scheme using the FHNC cluster summation technique. This makes feasible the microscopical investigation of heavy nuclei, such as ^{208}Pb. Isospin state dependence in the correlation can be safely handled and provides a better variational choice than Jastrow correlated wave functions. This encourages us to pursue the goal of a microscopic description of finite nuclei with even more realistic correlation functions and interactions containing, in particular, tensor components.

Aknowledgements This project has been partially supported by the CYCIT-INFN agreement and by the Junta de Andalucia. One of the authors (A.F.) wants to thank the warm hospitality of CEBAF, where part of the work has been done.

Appendix A

This appendix contains the two–body distribution function and one–body density FHNC equations for the j–j coupling and isospin dependence. The topological classification of the cluster diagrams (Nodal, Composite and Elementary, dd, de, ed and cc) has been already presented in Ref.[5], as well as the chaining technique; so it will not be repeated here.

In the following we shall indicate the coordinate $\mathbf{r}_i$ with i, and the convolution integral over the coordinate 3 as $(|)$.

The sums of the nodal diagrams $N^{\alpha\beta}_{xy=dd,de,ed,ee}$ are given by the solutions of the integral equations:

$$N^{\alpha\beta}_{xy}(1,2) = \sum_{\gamma=p,n}\sum_{x',y'=d,e}\left(X^{\alpha\gamma}_{xx'}(1,3)\xi^{\gamma}_{x'y'}(3) \mid N^{\gamma\beta}_{y'y}(3,2) + X^{\gamma\beta}_{y'y}(3,2)\right),$$

where $\xi^{\gamma}_{dd} = \xi^{\gamma}_{d}$, otherwise $\xi^{\gamma}_{xy} = \xi^{\gamma}_{e}$. The sum over $(x'y')$ runs over the pairs (dd, de, ed), because of the FHNC convolution rules.

The cc–chains now can contain the parallel exchange link $\rho^{\alpha}_{0,P}(1,2)$ and the antiparallel one $\rho^{\alpha}_{0,A}(1,2)$. We give here their explicit expressions, as they represent the main changes, due to the j–j coupling, respect to the usual symmetric matter FHNC Eqs.

$$\begin{aligned}
N^{(x)\alpha}_{cc,P}(1,2) &= \left(X^{\alpha}_{cc,P}(1,3)\xi^{\alpha}_{e}(3) \mid N^{\alpha}_{cc,P}(3,2) + X^{\alpha}_{cc,P}(3,2) - \rho^{\alpha}_{0,P}(3,2)\right) - \\
&\quad \left(X^{\alpha}_{cc,A}(1,3)\xi^{\alpha}_{e}(3) \mid N^{\alpha}_{cc,A}(3,2) + X^{\alpha}_{cc,A}(3,2) - \rho^{\alpha}_{0,A}(3,2)\right) \\
N^{(\rho)\alpha}_{cc,P}(1,2) &= -\left(\rho^{\alpha}_{0,P}(1,3)\xi^{\alpha}_{e}(3) \mid N^{(x)\alpha}_{cc,P}(3,2) + X^{\alpha}_{cc,P}(3,2)\right) \\
&\quad -\left(\rho^{\alpha}_{0,P}(1,3)(\xi^{\alpha}_{e}(3)-1) \mid N^{(\rho)\alpha}_{cc,P}(3,2) - \rho^{\alpha}_{0,P}(3,2)\right)
\end{aligned}$$

$$
\begin{aligned}
& + \Big(\rho^{\alpha}_{0,A}(1,3)\xi^{\alpha}_{e}(3) \mid N^{(x)\alpha}_{cc,A}(3,2) + X^{\alpha}_{cc,A}(3,2)\Big) \\
& + \Big(\rho^{\alpha}_{0,A}(1,3)(\xi^{\alpha}_{e}(3)-1) \mid N^{(\rho)\alpha}_{cc,A}(3,2) - \rho^{\alpha}_{0,A}(3,2)\Big) \\
N^{(x)\alpha}_{cc,A}(1,2) &= \Big(X^{\alpha}_{cc,A}(1,3)\xi^{\alpha}_{e}(3) \mid N^{\alpha}_{cc,P}(3,2) + X^{\alpha}_{cc,P}(3,2) - \rho^{\alpha}_{0,P}(3,2)\Big) + \\
& \Big(X^{\alpha}_{cc,P}(1,3)\xi^{\alpha}_{e}(3) \mid N^{\alpha}_{cc,A}(3,2) + X^{\alpha}_{cc,A}(3,2) - \rho^{\alpha}_{0,A}(3,2)\Big) \\
N^{(\rho)\alpha}_{cc,A}(1,2) &= -\Big(\rho^{\alpha}_{0,A}(1,3)\xi^{\alpha}_{e}(3) \mid N^{(x)\alpha}_{cc,P}(3,2) + X^{\alpha}_{cc,P}(3,2)\Big) \\
& - \Big(\rho^{\alpha}_{0,A}(1,3)(\xi^{\alpha}_{e}(3)-1) \mid N^{(\rho)\alpha}_{cc,P}(3,2) - \rho^{\alpha}_{0,P}(3,2)\Big) \\
& - \Big(\rho^{\alpha}_{0,P}(1,3)\xi^{\alpha}_{e}(3) \mid N^{(x)\alpha}_{cc,A}(3,2) + X^{\alpha}_{cc,A}(3,2)\Big) \\
& - \Big(\rho^{\alpha}_{0,P}(1,3)(\xi^{\alpha}_{e}(3)-1) \mid N^{(\rho)\alpha}_{cc,A}(3,2) - \rho^{\alpha}_{0,A}(3,2)\Big)\,,
\end{aligned}
$$

and

$$N^{\alpha}_{cc,X}(1,2) = N^{(x)\alpha}_{cc,X}(1,2) + N^{(\rho)\alpha}_{cc,X}(1,2).$$

The partial pair FHNC distribution functions, g_{xy}, and the sums of the composite diagrams, X_{xy}, are:

$$
\begin{aligned}
g^{\alpha\beta}_{dd}(1,2) &= f^{2}_{\alpha\beta}(1,2)\exp\Big[N^{\alpha\beta}_{dd}(1,2) + E^{\alpha\beta}_{dd}(1,2)\Big] \\
&= 1 + N^{\alpha\beta}_{dd}(1,2) + X^{\alpha\beta}_{dd}(1,2)
\end{aligned}
$$

$$
\begin{aligned}
g^{\alpha\beta}_{de}(1,2) &= g^{\beta\alpha}_{ed}(2,1) \\
&= g^{\alpha\beta}_{dd}(1,2)\Big[N^{\alpha\beta}_{de}(1,2) + E^{\alpha\beta}_{de}(1,2)\Big] \\
&= N^{\alpha\beta}_{de}(1,2) + X^{\alpha\beta}_{de}(1,2)
\end{aligned}
$$

$$
g^{\alpha\beta}_{ee}(1,2) = g^{\alpha\beta}_{dd}(1,2)\Big[N^{\alpha\beta}_{ee}(1,2) + E^{\alpha\beta}_{ee}(1,2) +
$$

$$
\begin{aligned}
& \Big(N^{\alpha\beta}_{ed}(1,2)+E^{\alpha\beta}_{ed}(1,2)\Big)\Big(N^{\alpha\beta}_{de}(1,2)+E^{\alpha\beta}_{de}(1,2)\Big)- \\
& 2\delta_{\alpha\beta}\Big(N^{\alpha}_{cc,P}(1,2)+E^{\alpha}_{cc,P}(1,2)-\rho^{\alpha}_{0,P}(1,2)\Big)^2- \\
& 2\delta_{\alpha\beta}\Big(N^{\alpha}_{cc,A}(1,2)+E^{\alpha}_{cc,A}(1,2)-\rho^{\alpha}_{0,A}(1,2)\Big)^2\Big] \\
= \;& N^{\alpha\beta}_{ee}(1,2)+X^{\alpha\beta}_{ee}(1,2)
\end{aligned}
$$

$$
\begin{aligned}
g^{\alpha}_{cc,X}(1,2) &= g^{\alpha\alpha}_{dd}(1,2)\Big[N^{\alpha}_{cc,X}(1,2)+E^{\alpha}_{cc,X}(1,2)-\rho^{\alpha}_{0,X}(1,2)\Big] \\
&= N^{\alpha}_{cc,X}(1,2)+X^{\alpha}_{cc,X}(1,2)-\rho^{\alpha}_{0,X}(1,2).
\end{aligned}
$$

The vertex corrections, $\xi^{\alpha}_{x=d,e}$, are given by:

$$
\begin{aligned}
\xi^{\alpha}_{e}(1) &= \exp\left[U^{\alpha}_{d}(1)\right] \\
\xi^{\alpha}_{d}(1) &= \xi^{\alpha}_{e}(1)\left[U^{\alpha}_{e}(1)+\rho^{\alpha}_{0}(1)\right],
\end{aligned}
$$

where

$$
\begin{aligned}
U^{\alpha}_{d}(1) &= \int d^3r_2 \sum_{\beta=p,n}\Big\{\xi^{\beta}_{d}(2)\Big[X^{\alpha\beta}_{dd}(1,2)-E^{\alpha\beta}_{dd}(1,2)-S^{\alpha\beta}_{dd}(1,2)\Big(g^{\alpha\beta}_{dd}(1,2)-1\Big)\Big]+ \\
&\quad \xi^{\beta}_{e}(2)\Big[X^{\alpha\beta}_{de}(1,2)-E^{\alpha\beta}_{de}(1,2)-S^{\alpha\beta}_{de}(1,2)\Big(g^{\alpha\beta}_{dd}(1,2)-1\Big)- \\
&\quad S^{\alpha\beta}_{dd}(1,2)g^{\alpha\beta}_{de}(1,2)\Big]\Big\}+E^{\alpha}_{d}(1) \\
U^{\alpha}_{e}(1) &= \int d^3r_2\Big\{ \sum_{\beta=p,n}\Big\{\xi^{\beta}_{d}(2)\Big[X^{\alpha\beta}_{ed}(1,2)-E^{\alpha\beta}_{ed}(1,2)-S^{\alpha\beta}_{ed}(1,2)\Big(g^{\alpha\beta}_{dd}(1,2)-1\Big)+ \\
&\quad S^{\alpha\beta}_{dd}(1,2)g^{\alpha\beta}_{ed}(1,2)\Big]+ \\
&\quad \xi^{\beta}_{e}(2)\Big[X^{\alpha\beta}_{ee}(1,2)-E^{\alpha\beta}_{ee}(1,2)-S^{\alpha\beta}_{ee}(1,2)\Big(g^{\alpha\beta}_{dd}(1,2)-1\Big)- \\
&\quad S^{\alpha\beta}_{ed}(1,2)g^{\alpha\beta}_{de}(1,2)-S^{\alpha\beta}_{de}(1,2)g^{\alpha\beta}_{ed}(1,2)-
\end{aligned}
$$

$$
\begin{aligned}
& S^{\alpha\beta}_{dd}(1,2) g^{\alpha\beta}_{ee}(1,2) \Big] \Big\} + \\
& 4\xi^{\alpha}_{e}(2) \Big[S^{\alpha}_{cc,P}(1,2) g^{\alpha}_{cc,P}(1,2) + S^{\alpha}_{cc,A}(1,2) g^{\alpha}_{cc,A}(1,2) \Big] - \\
& 2 \Big[\rho^{\alpha}_{0,P}(1,2) \Big(N^{(\rho)\alpha}_{cc,P}(1,2) - \rho^{\alpha}_{0,P}(1,2) \Big) + \\
& \quad \rho^{\alpha}_{0,A}(1,2) \Big(N^{(\rho)\alpha}_{cc,A}(1,2) - \rho^{\alpha}_{0,A}(1,2) \Big) \Big] \Big\} + E^{\alpha}_{e}(1),
\end{aligned}
$$

with:

$$
S^{\alpha\beta}_{xy}(1,2) = E^{\alpha\beta}_{xy}(1,2) + (1/2) N^{\alpha\beta}_{xy}(1,2)
$$

Notice that $\rho^{\alpha}_{1}(1) = \xi^{\alpha}_{d}(1)$.

Appendix B

Here we will shortly present the FHNC equations for the one–body density matrices $\rho^{ss'\alpha}(1,1')$. These are modifications of the equations presented in Ref.[6]. As we have discussed throught the text we have to separate the case with the same third component of spin

$$
\rho^{ss\alpha}(1,1') = -\xi^{\alpha}_{\omega}(1)\xi^{\alpha}_{\omega}(1') g^{\alpha}_{\omega\omega}(1,1') [N^{\alpha}_{\omega_c\omega_c,P}(1,1') + E^{\alpha}_{\omega_c\omega_c,P}(1,1') - \rho^{\alpha}_{0,P}(1,1')],
$$

from the case with different ones

$$
\rho^{s-s\alpha}(1,1') = -\xi^{\alpha}_{\omega}(1)\xi^{\alpha}_{\omega}(1') g^{\alpha}_{\omega\omega}(1,1') [N^{\alpha}_{\omega_c\omega_c,A}(1,1') + E^{\alpha}_{\omega_c\omega_c,A}(1,1') - \rho^{\alpha}_{0,A}(1,1')].
$$

$g^{\alpha}_{\omega\omega}$ is defined as:

$$
g^{\alpha}_{\omega\omega}(1,1') = \exp\Big[N^{\alpha}_{\omega\omega}(1,1') + E^{\alpha}_{\omega\omega}(1,1') \Big].
$$

The nodal functions $N^{\alpha}_{\omega\omega}, N^{\alpha}_{\omega_c\omega_c,X}$ are solutions of convolution equations, formally identical to those presented in appendix A, with the substitution of the external $(1,2)$ link indices (d,c) by (ω,ω_c), where needed. New nodal terms $N^{\alpha\beta}_{\omega d,\omega e}, N^{\alpha\beta}_{\omega_c c,X}$ appear in these convolutions. The same rule as before applies to them.

New partial FHNC distribution functions need to be introduced. They are given by:

$$\begin{aligned} g^{\alpha\beta}_{\omega d}(1,2) &= g^{\beta\alpha}_{d\omega}(2,1) \\ &= f_{\alpha\beta}(1,2)\exp\Big[N^{\alpha\beta}_{\omega d}(1,2)+E^{\alpha\beta}_{\omega d}(1,2)\Big] \\ &= 1+N^{\alpha\beta}_{\omega d}(1,2)+X^{\alpha\beta}_{\omega d}(1,2) \end{aligned}$$

$$\begin{aligned} g^{\alpha\beta}_{\omega e}(1,2) &= g^{\beta\alpha}_{e\omega}(2,1) \\ &= g^{\alpha\beta}_{\omega d}(1,2)\Big[N^{\alpha\beta}_{\omega e}(1,2)+E^{\alpha\beta}_{\omega e}(1,2)\Big] \\ &= N^{\alpha\beta}_{\omega e}(1,2)+X^{\alpha\beta}_{\omega e}(1,2) \end{aligned}$$

$$\begin{aligned} g^{\alpha\alpha}_{\omega_c c,X}(1,2) &= g^{\alpha\alpha}_{\omega d}(1,2)\Big[N^{\alpha\alpha}_{\omega_c c,X}(1,2)+E^{\alpha\alpha}_{\omega_c c,X}(1,2)-\rho^{\alpha}_{0,X}(1,2)\Big] \\ &= N^{\alpha\alpha}_{\omega_c c,X}(1,2)+X^{\alpha\alpha}_{\omega_c c,X}(1,2)-\rho^{\alpha}_{0,X}(1,2). \end{aligned}$$

The vertex corrections, ξ^{α}_{ω}, is:

$$\xi^{\alpha}_{\omega}(1)=\exp\left[U^{\alpha}_{\omega}(1)\right],$$

with:

$$U^{\alpha}_{\omega}(1) = \int d^3r_2 \sum_{\beta=p,n}\Big\{\xi^{\beta}_{d}(2)\Big[X^{\alpha\beta}_{\omega d}(1,2)-E^{\alpha\beta}_{\omega d}(1,2)-S^{\alpha\beta}_{\omega d}(1,2)\Big(g^{\alpha\beta}_{\omega d}(1,2)-1\Big)\Big]+$$

$$\xi_e^\beta(2)\Big[X_{\omega e}^{\alpha\beta}(1,2) - E_{\omega e}^{\alpha\beta}(1,2) - S_{\omega e}^{\alpha\beta}(1,2)\left(g_{\omega d}^{\alpha\beta}(1,2) - 1\right) -$$

$$S_{\omega d}^{\alpha\beta}(1,2) g_{\omega e}^{\alpha\beta}(1,2)\Big]\Big\} + E_\omega^\alpha(1).$$

Appendix C

In this appendix, we shall give the explicit expressions for the uncorrelated one–body densities and related quantities. For the s.p. wavefunctions we use:

$$\phi_{nljm}^\alpha(\vec{x}_i) = R_{nlj}^\alpha(r_i)\sum_{\mu,s}\langle l\mu\frac{1}{2}s \mid jm\rangle Y_{l\mu}(\hat{r}_i)\chi_s(i)\chi_\alpha(i)$$

The one–body density ρ_{T1}^α is given by:

$$\rho_{T1}^\alpha(\mathbf{r}_1) = \frac{1}{4\pi}\sum_{nlj}(2j+1)\left[R_{nlj}^\alpha(r_1)\left(D_{nlj}^\alpha(r_1) - \frac{l(l+1)}{r_1^2}R_{nlj}^\alpha(r_1)\right) - (R_{nlj}^\alpha(r_1)')^2\right]$$

where we have defined:

$$D_{nlj}^\alpha(r_1) = \nabla_1^2 R_{nlj}^\alpha(r_1) = R_{nlj}^{\alpha\prime\prime}(r_1) + \frac{2}{r_1}R_{nlj}^{\alpha\prime}(r_1) - \frac{l(l+1)}{r_1^2}R_{nlj}^\alpha(r_1).$$

For the one–body density matrix ρ_{T2}^α we find:

$$\begin{aligned}
\rho_{T2}^\alpha(\mathbf{r}_1,\mathbf{r}_2) = & \frac{1}{2(4\pi)^2}\sum_{\substack{nlj\\ n'l'j'}}(2j+1)(2j'+1)R_{nlj}^\alpha(r_2)R_{n'l'j'}^\alpha(r_2)\\
& \Big\{\Big[R_{nlj}^\alpha(r_1)D_{n'l'j'}^\alpha(r_1) - R_{nlj}^{\alpha\prime}(r_1)R_{n'l'j'}^{\alpha\prime}(r_1)\Big]P_l(\cos\theta)P_{l'}(\cos\theta) -\\
& \frac{\sin^2\theta}{r_1^2}R_{nlj}^\alpha(r_1)R_{n'l'j'}^\alpha(r_1)P_l'(\cos\theta)P_{l'}'(\cos\theta)\Big\} +\\
& \frac{2}{(4\pi)^2}\sum_{\substack{nlj\\ n'l'j'}}(-1)^{j+j'-l-l'-1}R_{nlj}^\alpha(r_2)R_{n'l'j'}^\alpha(r_2)\\
& \Big\{\Big[R_{nlj}^\alpha(r_1)D_{n'l'j'}^\alpha(r_1) - R_{nlj}^{\alpha\prime}(r_1)R_{n'l'j'}^{\alpha\prime}(r_1)\Big]Q_l(\cos\theta)Q_{l'}(\cos\theta) -\\
& \frac{\sin^2(\theta)}{r_1^2}R_{nlj}^\alpha(r_1)R_{n'l'j'}^\alpha(r_1)Q_l'(\cos\theta)Q_{l'}'(\cos\theta)\Big\},
\end{aligned}$$

where P_l are Legendre polynomials, θ is the angle between the vectors $\mathbf{r}_1$ and $\mathbf{r}_2$ and we have defined:

$$\begin{aligned} Q_l(\cos\theta) &= \sin\theta P_l'(\cos\theta) \\ Q_l'(\cos\theta) &= \frac{1}{\sin\theta}\left(\cos\theta P_l'(\cos\theta) - l(l+1)P_l(\cos\theta)\right). \end{aligned}$$

For the T_3 densities we obtain:

$$\begin{aligned} \rho^{\alpha}_{T3,P}(\mathbf{r}_1,\mathbf{r}_2) &= 2\nabla_1^2\rho^{\alpha}_{0,P}(\mathbf{r}_1,\mathbf{r}_2) = \frac{1}{4\pi}\sum_{nlj}(2j+1)R^{\alpha}_{nlj}(r_2)D^{\alpha}_{nlj}(r_1)P_l(\cos\theta) \\ \rho^{\alpha}_{T3,A}(\mathbf{r}_1,\mathbf{r}_2) &= 2\nabla_1^2\rho^{\alpha}_{0,A}(\mathbf{r}_1,\mathbf{r}_2) = \frac{1}{2\pi}\sum_{nlj}(-1)^{j-l-1/2}R^{\alpha}_{nlj}(r_2)D^{\alpha}_{nlj}(r_1)Q_l(\cos\theta). \end{aligned}$$

Finally, ρ^{α}_{T4}, appearing in the calculation of the center of mass term T_{cm}, is given by:

$$\rho^{\alpha}_{T4}(\mathbf{r}_1,\mathbf{r}_2) = \rho^{\alpha}_{T6}(\mathbf{r}_1,\mathbf{r}_2) - \rho^{\alpha}_{0,P}(\mathbf{r}_1,\mathbf{r}_2)\rho^{\alpha}_{T5,P}(\mathbf{r}_1,\mathbf{r}_2) - \rho^{\alpha}_{0,A}(\mathbf{r}_1,\mathbf{r}_2)\rho^{\alpha}_{T5,A}(\mathbf{r}_1,\mathbf{r}_2),$$

where

$$\begin{aligned} \rho^{\alpha}_{T6}(\mathbf{r}_1,\mathbf{r}_2) &= 2\left(\nabla_1\rho^{\alpha}_{0,P}(\mathbf{r}_1,\mathbf{r}_2)\cdot\nabla_2\rho^{\alpha}_{0,P}(\mathbf{r}_1,\mathbf{r}_2) + \nabla_1\rho^{\alpha}_{0,A}(\mathbf{r}_1,\mathbf{r}_2)\cdot\nabla_2\rho^{\alpha}_{0,A}(\mathbf{r}_1,\mathbf{r}_2)\right), \\ \rho^{\alpha}_{T5,X}(\mathbf{r}_1,\mathbf{r}_2) &= 2\nabla_1\cdot\nabla_2\rho^{\alpha}_{0,X}(\mathbf{r}_1,\mathbf{r}_2), \end{aligned}$$

and

$$\begin{aligned} \rho^{\alpha}_{T5,P}(\mathbf{r}_1,\mathbf{r}_2) &= \frac{1}{4\pi}\sum_{nlj}(2j+1)\Bigg[R^{\alpha\prime}_{nlj}(r_1)R^{\alpha\prime}_{nlj}(r_2)\cos\theta P_l(\cos\theta) + \\ &\left(R^{\alpha}_{nlj}(r_2)\frac{R^{\alpha}_{nlj}(r_1)}{r_1} + R^{\alpha}_{nlj}(r_1)\frac{R^{\alpha}_{nlj}(r_2)}{r_2}\right)\sin^2\theta P_l'(\cos\theta) + \\ &\frac{R^{\alpha}_{nlj}(r_1)R^{\alpha}_{nlj}(r_2)}{r_1r_2}\left(\sin^2\theta P_l'(\cos\theta) + l(l+1)\cos\theta P_l(\cos\theta)\right)\Bigg] \\ \rho^{\alpha}_{T5,A}(\mathbf{r}_1,\mathbf{r}_2) &= \frac{1}{2\pi}\sum_{nlj}(-1)^{j-l-1/2}\Bigg[R^{\alpha\prime}_{nlj}(r_1)R^{\alpha\prime}_{nlj}(r_2)\cos\theta Q_l(\cos\theta) + \end{aligned}$$

$$
\begin{aligned}
&\left(R^{\alpha}_{nlj}(r_2)\frac{R^{\alpha}_{nlj}(r_1)}{r_1} + R^{\alpha}_{nlj}(r_1)\frac{R^{\alpha}_{nlj}(r_2)}{r_2}\right)\sin^2\theta Q'_l(\cos\theta) \\
&\frac{R^{\alpha}_{nlj}(r_1)R^{\alpha}_{nlj}(r_2)}{r_1 r_2}\Big\{\sin^2\theta Q'_l(\cos\theta)+ \\
&\left(l(l+1)-\frac{1}{\sin^2\theta}\right)\cos\theta Q_l(\cos\theta)\Big\}\Big] \\
\rho^{\alpha}_{T6}(\mathbf{r}_1,\mathbf{r}_2) \quad = \quad &\frac{1}{2(4\pi)^2}\sum_{\substack{nlj\\ n'l'j'}}(2j+1)(2j'+1)R^{\alpha}_{nlj}(r_2)R^{\alpha}_{n'l'j'}(r_1) \\
&\Big\{\cos\theta\Big[R^{\alpha\prime}_{nlj}(r_2)R^{\alpha\prime}_{n'l'j'}(r_1)P_l(\cos\theta)P_{l'}(\cos\theta) - \\
&\sin^2\theta\frac{R^{\alpha}_{nlj}(r_2)R^{\alpha}_{n'l'j'}(r_1)}{r_1 r_2}P'_l(\cos\theta)P'_{l'}(\cos\theta)\Big] + \\
&\sin^2\theta\Big[\frac{R^{\alpha}_{nlj}(r_2)}{r_2}R^{\alpha\prime}_{n'l'j'}(r_1)P'_l(\cos\theta)P_{l'}(\cos\theta) + \\
&R^{\alpha\prime}_{nlj}(r_2)\frac{R^{\alpha}_{n'l'j'}(r_1)}{r_1}P_l(\cos\theta)P'_{l'}(\cos\theta)\Big]\Big\} \\
&\frac{2}{(4\pi)^2}\sum_{\substack{nlj\\ n'l'j'}}(-1)^{j+j'-l-l'-1}R^{\alpha}_{nlj}(r_2)R^{\alpha}_{n'l'j'}(r_1) \\
&\Big\{\cos\theta\Big[R^{\alpha\prime}_{nlj}(r_2)R^{\alpha\prime}_{n'l'j'}(r_1)f_l(\cos\theta)f_{l'}(\cos\theta) - \\
&\sin^2\theta\frac{R^{\alpha}_{nlj}(r_2)R^{\alpha}_{n'l'j'}(r_1)}{r_1 r_2}f'_l(\cos\theta)f'_{l'}(\cos\theta)\Big] + \\
&\sin^2\theta\Big[\frac{R^{\alpha}_{nlj}(r_2)}{r_2}R^{\alpha\prime}_{n'l'j'}(r_1)f'_l(\cos\theta)f_{l'}(\cos\theta) + \\
&R^{\alpha\prime}_{nlj}(r_2)\frac{R^{\alpha}_{n'l'j'}(r_1)}{r_1}f_l(\cos\theta)f'_{l'}(\cos\theta)\Big]\Big\}.
\end{aligned}
$$

References

[1] V.R.Pandharipande, "Proceedings of Cargèse summer School 1989", J. Tran Tranh Van and J. Negele Ed.s (Plenum Press, NY 1990).

[2] C.R.Chen, G.L.Payne, J.L.Payne and B.F.Gibson, Phys. Rev. **C33** (1986) 1740; J.Carlson, Phys. Rev. **C36** (1987) 2026; A.Stadler, W.Glöckle and P.U.Sauer, Phys. Rev. **C44** (1991) 2319; A.Kievsky, M.Viviani and S.Rosati, Nucl. Phys. **A551** (1993) 241.

[3] R.B.Wiringa, V.Fiks and A.Fabrocini, Phys. Rev. **C38** (1988) 1010.

[4] M.Baldo, I.Bombaci, S.Ferreira, G.Giansiracusa and U. Lombardo, Phys. Rev. **C43** (1991) 2605.

[5] G. Co', A. Fabrocini, S. Fantoni and I. E.. Lagaris, Nucl. Phys. **A549**(1992) 439.

[6] G. Co', A. Fabrocini and S. Fantoni, Nucl. Phys. **A568** (1994) 73.

[7] V.R.P. Pandharipande and R.B. Wiringa, Rev. Mod. Phys. **51** (1979) 821; S. Rosati in: From nuclei to particles, Proc. Int. School E. Fermi, course LXXIX, ed A. Molinari (North–Holland, Amsterdam, 1982).

[8] S. Fantoni and S. Rosati, Phys.Lett. **B84** (1979) 23.

[9] G.Rinker and J.Speth, Nucl. Phys. **A306** (1978) 360. G.Co' and S. Krewald, Phys. Lett. **B127** (1984) 145.

G.Co', A.M. Lallena and T.W.Donnelly, Nucl. Phys. **A469** (1987) 684.

J.E.Amaro and A.M.Lallena, Nucl. Phys. **A537** (1992) 585.

[10] F.Arias de Saavedra, Ph.D.Thesis, Universidad de Granada (1992), unpublished.

[11] I.R.Afnan and Y.C.Tang, Phys.Rev. **175** (1968) 1337.

[12] R.Guardiola, A.Faessler, H. Müther and A. Polls, Nucl. Phys. **A371** (1981) 79.

[13] S.C.Pieper, V.R.Pandharipande and R.B.Wiringa, Phys.Rev. **C46** (1992) 1741.

[14] D.M.Brink and E.Boeker, Nucl.Phys. **A91** (1967) 1.

[15] R.B.Wiringa, private communication.

Tables

	q	$a_q^{\alpha\beta}$	$b_q^{\alpha\beta}$	$c_q^{\alpha\beta}$
	1	1	1	1
	2	0	3	-1
$\alpha = \beta$	3	1	1	1
	4	0	3	-1
	1	1	0	0
	2	0	0	0
$\alpha \neq \beta$	3	-1	2	2
	4	0	6	-2

Table 1. Coefficients of eq.(25).

	^{12}C	^{16}O	^{40}Ca	^{48}Ca	^{208}Pb
S_p	0.999	1.000	1.000	1.000	0.995
S_n	0.999	1.000	1.000	0.999	0.996
S_{pp}	0.994	0.998	1.000	0.999	0.989
S_{np}	0.998	1.000	1.000	0.999	0.991
S_{nn}	0.994	0.997	1.000	0.998	0.993
$S_{\sigma,0}$	1.004	1.018	1.009	1.014	0.953
$S_{\sigma,1}$	1.001	1.000	1.000	1.002	0.985

Table 2. Ground state sum rules. $S_{\sigma,0(1)}$ are the ratios $S_\sigma^{corr}/S_\sigma^{unc}$ in FHNC/0 and FHNC–1 approximations, respectively (see text).

	V_0	R	a
^{12}C	52.5	3.20	0.53
^{16}O	52.5	3.20	0.53
^{40}Ca	57.5	4.10	0.53
^{48}Ca	57.5	4.10	0.53
^{208}Pb	60.4	7.46	0.79

Table 3. Coefficients of the Woods–Saxon potential (56) used for the calculations of Tab.4.

^{12}C	F1	F2	F3	F4
V	-21.28	-21.43	-21.43	-21.24
V_C	0.00	0.00	0.64	0.63
T	19.10	19.28	19.28	19.09
E	-2.18	-2.15	-1.51	-1.52
^{16}O	F1	F2	F3	F4
V	-26.18	-26.18	-26.18	-25.84
V_C	0.00	0.00	0.87	0.86
T	20.16	20.16	20.16	19.87
E	-6.02	-6.02	-5.15	-5.11
^{40}Ca	F1	F2	F3	F4
V	-32.61	-32.61	-32.61	-31.97
V_C	0.00	0.00	1.95	1.91
T	23.96	23.96	23.96	23.45
E	-8.65	-8.65	-6.70	-6.61
^{48}Ca	F1	F2	F3	F4
V	-33.41	-33.69	-33.69	-32.13
V_C	0.00	0.00	1.62	1.59
T	25.77	26.12	26.12	25.68
E	-7.64	-7.57	-5.95	-5.86
^{208}Pb	F1	F2	F3	F4
V	-33.44	-33.70	-33.70	-32.67
V_C	0.00	0.00	3.98	3.84
T	24.04	24.29	24.29	23.68
E	-9.40	-9.41	-5.43	-5.15

Table 4. Energies per nucleon, in MeV, for the five nuclei considered. These results have been obtained using the Woods–Saxon parameters of Tab.3, the S3 interaction of Afnan and Tang [11] and the Euler ACA correlation. The healing distances are $d = 2.1 fm$ for ^{12}C and $d = 2.0 fm$ for the other nuclei.

		V_0	V_{LS}	R	a
^{12}C	p	62.00	3.20	2.86	0.57
	n	60.00	3.15	2.86	0.57
^{16}O	p	52.50	7.00	3.20	0.53
	n	52.50	6.54	3.20	0.53
^{40}Ca	p	57.50	11.11	4.10	0.53
	n	55.00	8.50	4.10	0.53
^{48}Ca	p	59.50	8.55	4.36	0.53
	n	50.00	7.74	4.36	0.53
^{208}Pb	p	60.40	6.75	7.46	0.79
	n	44.32	6.08	7.46	0.66

Table 5. Coefficients of the Woods–Saxon potential (56).

		$< V >$	$< V_c >$	T_ϕ	T_F	T_{cm}	$< H >$	E/A	d
	EU	-335.5	8.2	228.7	65.4	12.8	-33.2	-3.84	2.44
^{12}C	ACA	-291.9	8.2	223.2	45.0	12.8	-15.5	-2.36	2.20
	G	-273.2	8.0	221.3	31.3	12.8	-12.6	-2.12	
	EU	-489.5	14.4	273.3	82.1	11.4	-119.7	-8.20	2.36
^{16}O	ACA	-418.5	13.9	266.8	55.0	11.4	-82.8	-5.89	2.08
	G	-395.8	13.5	263.2	43.4	11.4	-75.7	-5.44	
	EU	-1515.1	80.4	791.3	262.6	10.1	-381.2	-9.78	2.42
^{40}Ca	ACA	-1302.2	78.0	771.9	190.2	10.1	-262.1	-6.81	2.20
	G	-1220.0	75.6	750.3	154.2	10.1	-239.9	-6.25	
	EU	-1744.9	78.8	968.8	302.4	9.6	-394.9	-8.43	2.45
^{48}Ca	ACA	-1494.5	76.0	936.6	209.6	9.6	-272.3	-5.87	2.15
	G	-1418.8	74.3	918.7	182.7	9.6	-243.2	-5.27	
	EU	-7600.3	810.8	3865.3	1163.6	6.0	-1761.4	-8.50	2.52
^{208}Pb	ACA	-6772.0	809.2	3910.7	995.8	6.0	-1056.3	-5.11	2.45
	G	-6218.4	792.1	3740.7	814.1	6.0	-871.5	-4.22	

Table 6. Ground state expectation values with different correlations. EU indicates the Euler correlation, ACA the ACA Euler correlation and G the ACA gaussian correlation. The parameters of the gaussian correlations are $A = 0.7$ for all the nuclei considered and $B = 2.15 fm^{-2}$ for ^{48}Ca, $B = 2.2 fm^{-2}$ for ^{12}C, ^{40}Ca and ^{208}Pb, and $B = 2.3 fm^{-2}$ for ^{16}O. $T_\phi = T_\phi^{(1)} + T_\phi^{(2)} + T_\phi^{(3)}$. Energies in MeV and distances in fm.

	$< V >$	$< V_c >$	T_ϕ	T_F	T_{cm}	$< H >$	E/A	d
^{12}C	-293.6	8.1	221.9	15.6	12.8	-48.0	-5.07	2.17
^{16}O	-435.0	13.6	252.4	20.9	11.4	-136.7	-9.26	2.07
^{40}Ca	-1328.6	76.7	759.2	78.2	10.1	-414.5	-10.62	2.25
^{48}Ca	-1554.1	75.6	931.1	93.2	9.6	-454.2	-9.66	2.30
^{208}Pb	-7017.8	805.3	3827.5	390.2	6.0	-1994.8	-9.62	2.50

Table 7. Ground state energies for the ACA Euler correlation and the B1 potential. Energies in MeV and distances in fm.

	$S3$		$B1$	
	E_1	Δ	E_1	Δ
^{12}C	-2.21	6.36	-4.63	8.68
^{16}O	-5.57	5.43	-8.61	7.02
^{40}Ca	-6.33	7.04	-10.05	5.37
^{48}Ca	-5.28	10.05	-9.33	3.42
^{208}Pb	-5.14	-0.59	-9.69	-0.73

Table 8. FHNC–1 binding energies per nucleon calculated with the Euler–ACA correlations for the S3 and B1 interactions. Δ is the percentile deviation from the FHNC/0 energy.

		MD_0^p/x_p	MD_0^n/x_n	$MD_2/<T>$
^{12}C	EU	0.990	0.990	0.955
	ACA	0.995	0.995	0.960
	G	0.997	0.997	0.942
^{16}O	EU	0.996	0.996	0.969
	ACA	0.996	0.996	0.963
	G	0.996	0.996	0.954
^{40}Ca	EU	1.000	0.995	0.956
	ACA	0.995	0.996	0.942
	G	0.992	0.993	0.919
^{48}Ca	EU	0.998	0.993	0.949
	ACA	0.993	0.994	0.936
	G	0.991	0.993	0.914
^{208}Pb	EU	0.999	1.005	0.943
	ACA	0.996	1.002	0.934
	G	0.984	0.985	0.917

Table 9. Momentum distributions SRs, Eqs.(37,38), for the calculation of Tab.6. $x_p = Z/A$ and $x_n = N/A$ are the proton and neutron concentrations respectively.

Figure captions

Fig.1. ACA Euler (upper panel) and gaussian (lower panel) correlation functions at the energy minimum for several nuclei, for the S3 potential.

Fig.2. Euler and ACA Euler correlation functions at the energy minimum for ^{12}C and ^{48}Ca nuclei with the S3 interaction. Full lines are the ACA Euler correlations. The lowest panel gives the nuclear matter $nn(=pp)$ (dot–dashed) and np (dashed) Euler correlations fot the same potential, at $d = 2.0fm$.

Fig.3. Proton density distributions. Full lines are the uncorrelated densities. The dotted curves are obtained with the ACA gaussian correlation, the dashed curves with the ACA Euler correlation and the dot–dashed curves with the isospin dependent Euler ones. The S3 interaction has been used. The dash-doubly-dotted curves are the densities obtained with the B1 potential using the ACA Euler correlation.

Fig.4. Proton momentum distributions. Curves as in Fig.3.

Fig. 5. Proton density (upper panel) and momentum distribution (lower panel) for ^{208}Pb. Curves as in Fig.3.

Fig. 6. ACA Euler correlation functions for the B1 interaction.

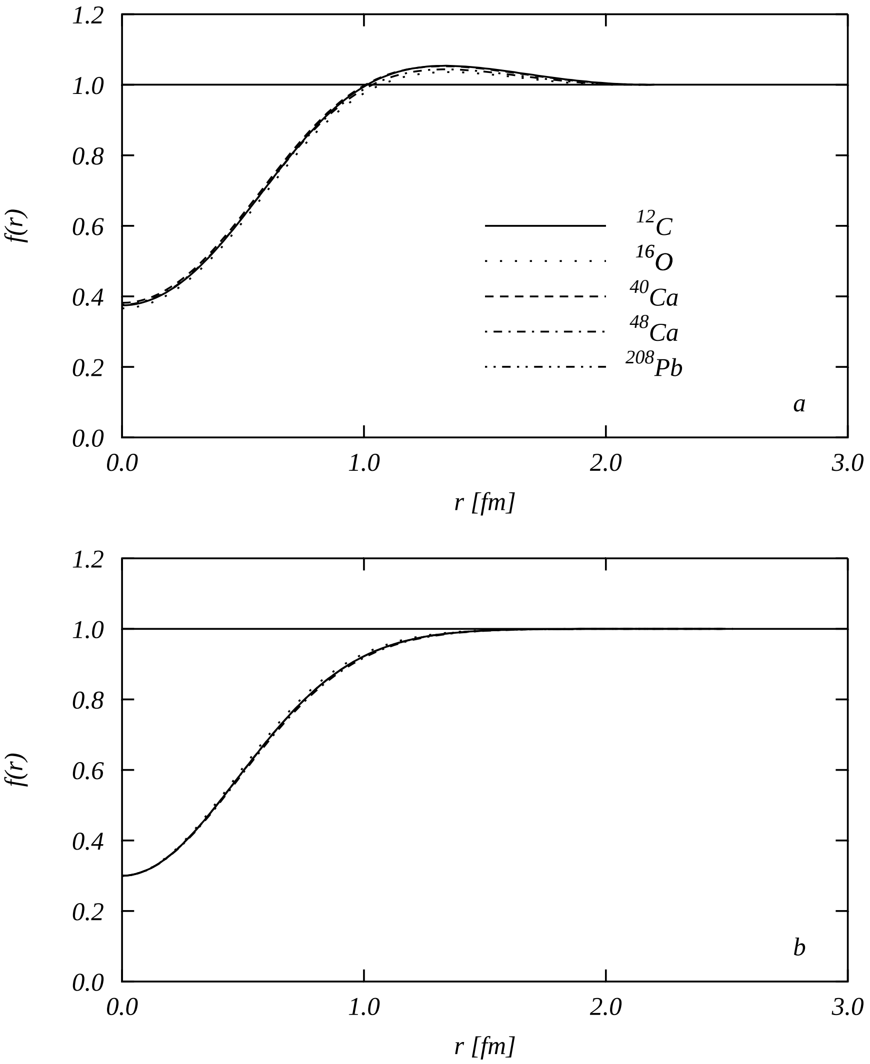

f(r)
r [fm]
0.0
0.2
0.4
0.6
0.8
1.0
1.2
1.0
2.0
3.0
12C
16O
40Ca
48Ca
208Pb
a
b

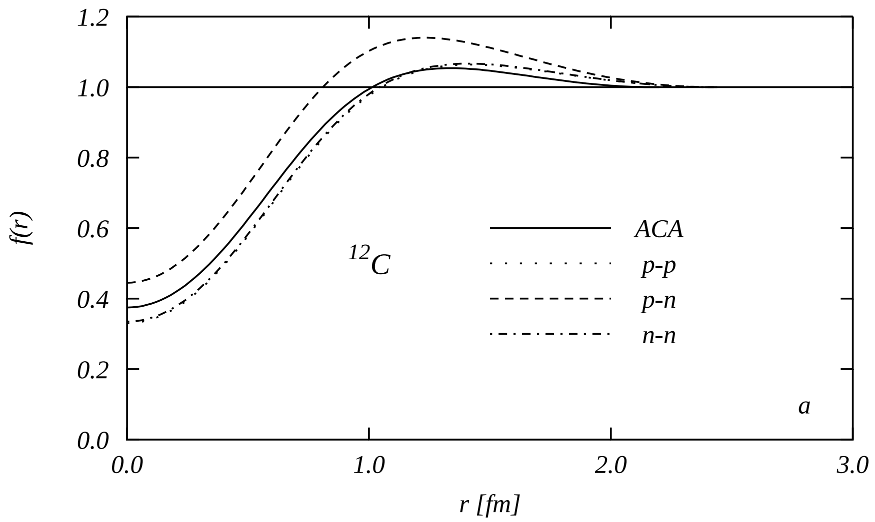

1.2
1.0
0.8
0.6
0.4
0.2
0.0
f(r)
^{12}C
ACA
p-p
p-n
n-n
a
0.0
1.0
2.0
3.0
r [fm]

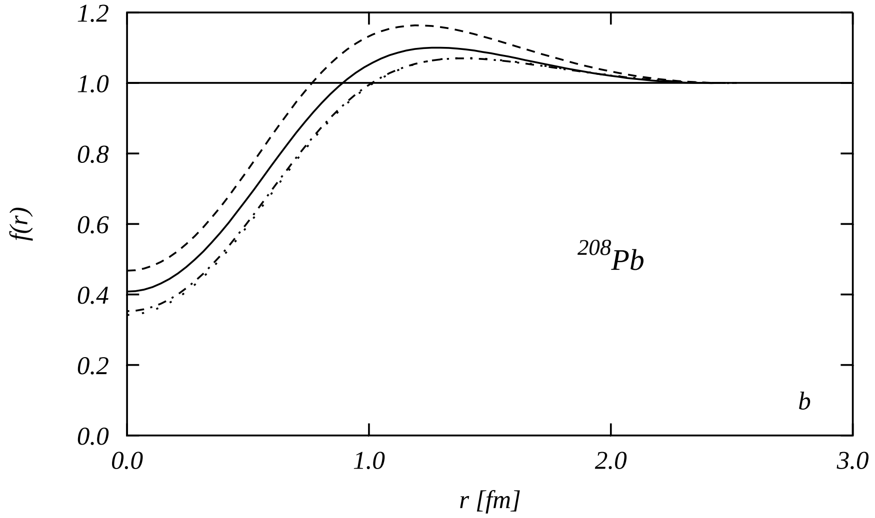

1.2
1.0
0.8
0.6
0.4
0.2
0.0
f(r)
^{208}Pb
b
0.0
1.0
2.0
3.0
r [fm]

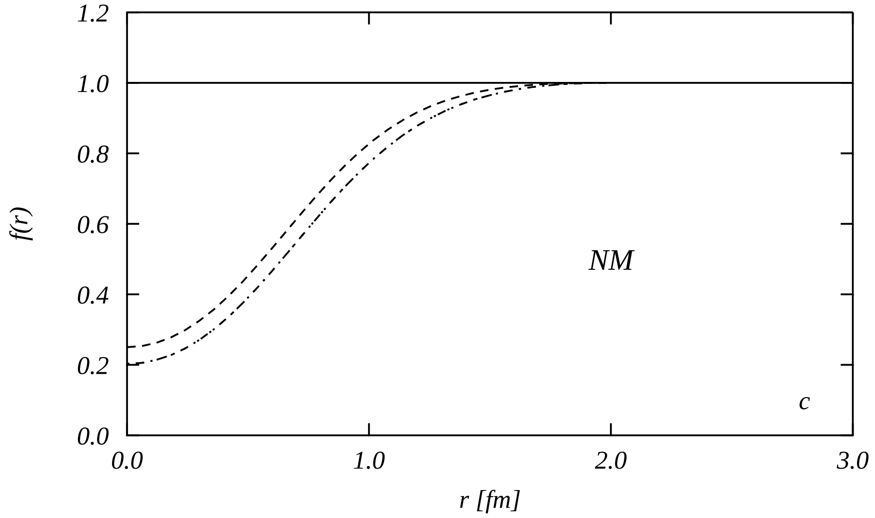

1.2
1.0
0.8
0.6
0.4
0.2
0.0
f(r)
NM
c
0.0
1.0
2.0
3.0
r [fm]

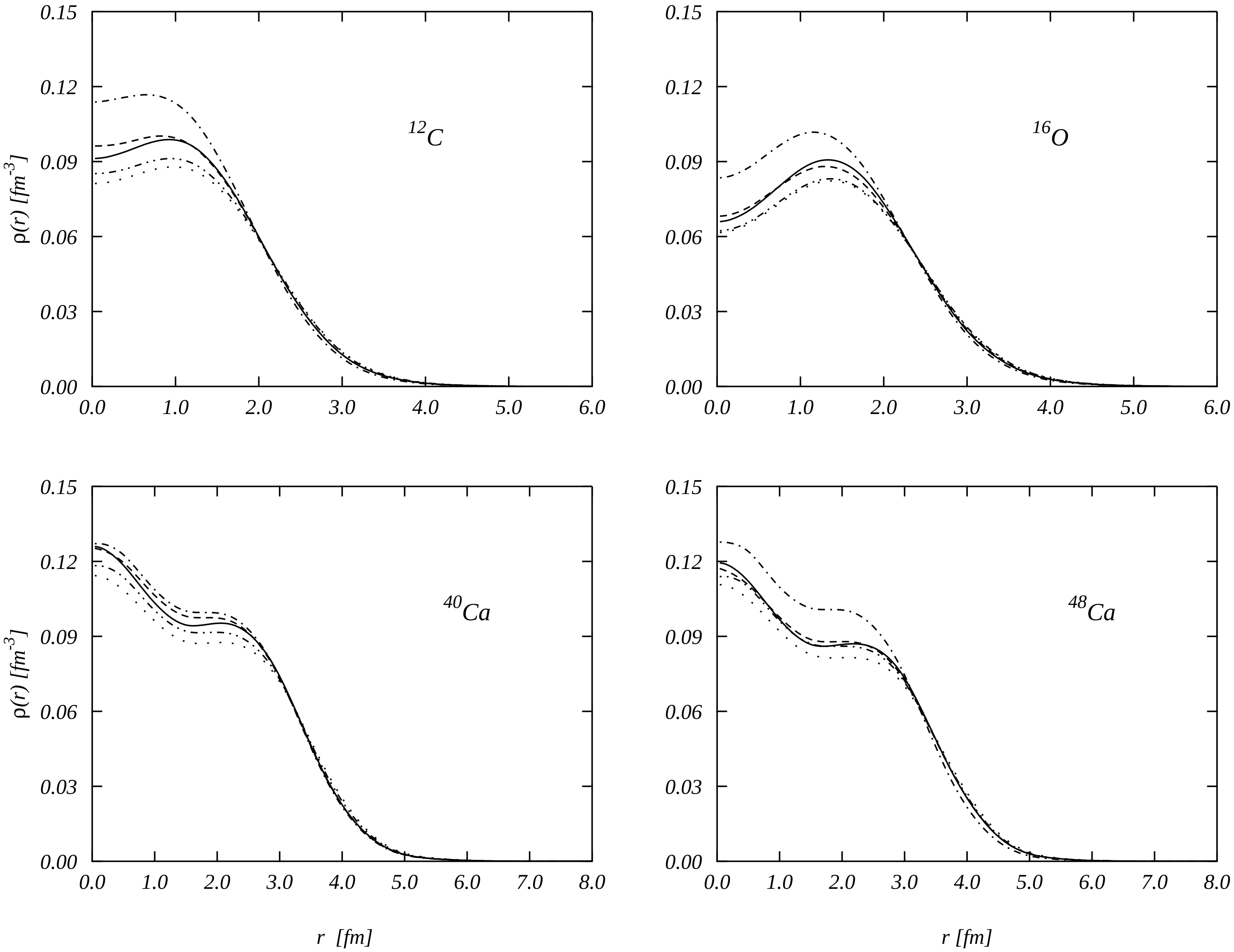

^{12}C
^{16}O
^{40}Ca
^{48}Ca
ρ(r) [fm^{-3}]
r [fm]
0.00
0.03
0.06
0.09
0.12
0.15
0.0
1.0
2.0
3.0
4.0
5.0
6.0
7.0
8.0

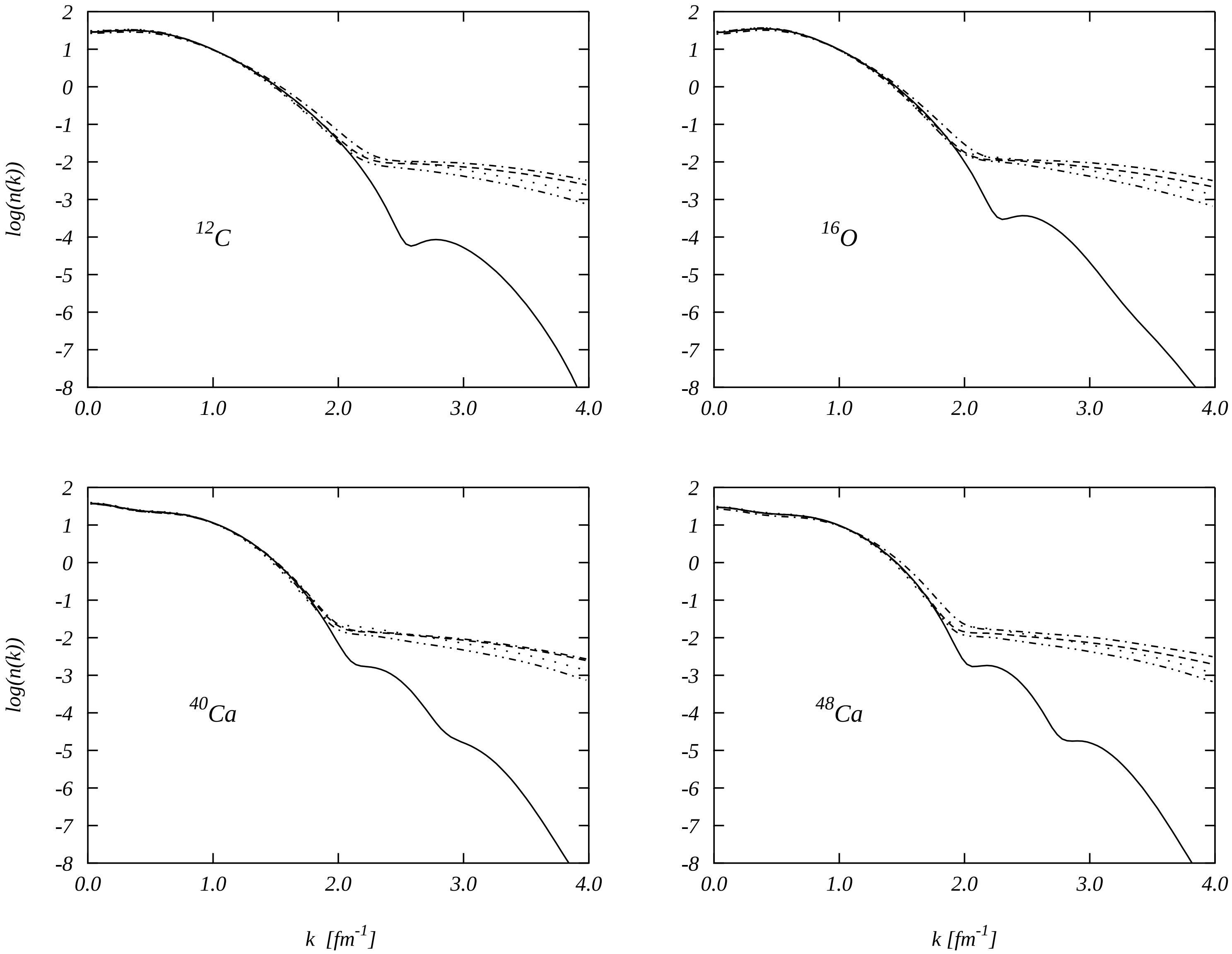

log(n(k))
12C
16O
40Ca
48Ca
k [fm-1]

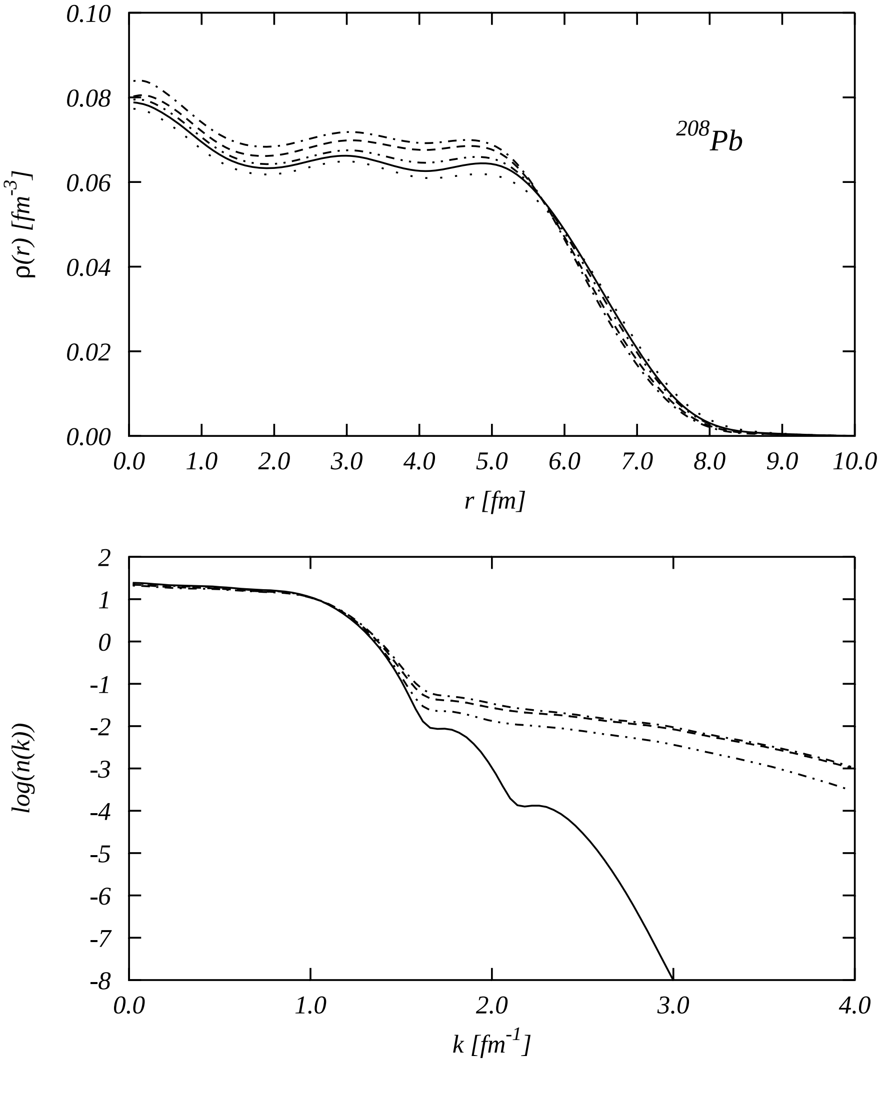

0.10
0.08
0.06
0.04
0.02
0.00
ρ(r) [fm^-3]
208Pb
0.0 1.0 2.0 3.0 4.0 5.0 6.0 7.0 8.0 9.0 10.0
r [fm]
2
1
0
-1
-2
-3
-4
-5
-6
-7
-8
log(n(k))
0.0 1.0 2.0 3.0 4.0
k [fm^-1]

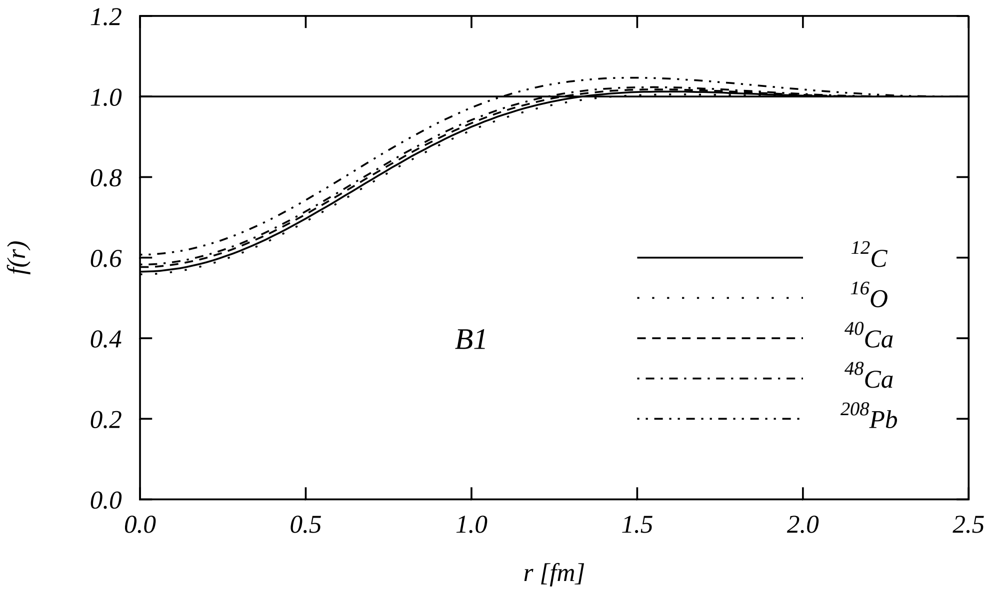
f(r)
r [fm]
B1
12C
16O
40Ca
48Ca
208Pb